Simultaneous measurements of $(\vec{p},\vec{p}')$ and $(\vec{p},p'\gamma)$ observables for the 15.11 MeV, 1^+, $T=1$ state in ^{12}C at 200 MeV

S. P. Wells,* S. W. Wissink, A. D. Bacher, G. P. A. Berg, S. M. Bowyer,† S. Chang, W. A. Franklin, J. Liu, and E. J. Stephenson
Indiana University Cyclotron Facility, Bloomington, Indiana 47408

J. R. Beene, F. E. Bertrand, M. L. Halbert, P. E. Mueller, D. H. Olive,‡ D. W. Stracener, and R. L. Varner
Oak Ridge National Laboratory, Oak Ridge, Tennessee 37831

J. Lisantti
Centenary College of Louisiana, Shreveport, Louisiana 71134

K. H. Hicks
Ohio University, Athens, Ohio 45701
(Received 21 July 1995)

We have made simultaneous measurements of singles $(\vec{p},\vec{p}')$ spin-transfer observables and coincident $(\vec{p},p'\gamma)$ yields and asymmetries for the 15.11 MeV, 1^+, $T=1$ state in ^{12}C, at an incident proton bombarding energy of 200 MeV. Data were taken at four proton scattering angles ranging from $\theta_p^{\text{c.m.}}=5.5°$ to 16.5°. Both vertical (normal to the reaction plane) and horizontal (in-plane) incident beam polarizations were used, which allowed us to extract 16 different observables for this transition. In particular, using the $(\vec{p},p'\gamma)$ reaction, we measured the sideways and longitudinal analyzing powers, D_{0S} and D_{0L}, which vanish identically in the $(\vec{p},p')$ reaction. Detailed comparisons of all observables to calculations done in both relativistic and nonrelativistic formalisms are presented. Surprisingly, a relativistic description in which knock-on exchange processes are not explicitly included provides the best overall agreement with the data.

PACS number(s): 25.40.Ep, 24.70.+s, 25.90.+k

I. INTRODUCTION AND MOTIVATION

The scattering of nucleons from nuclei can provide valuable information about both the nuclear force and the structure of the nucleus in which this force acts. In the intermediate energy regime (~150–500 MeV), where the impulse approximation is generally considered a valid reaction model, much of our knowledge as to how the free nucleon-nucleon (NN) interaction is modified by the presence of the nuclear medium has been obtained through measurements of $(\vec{p},\vec{p}')$ spin-transfer observables, for transitions to either discrete nuclear states [1] or to the continuum via quasielastic scattering [2]. In these types of singles $(\vec{p},\vec{p}')$ measurements, however, no more than eight independent quantities can be measured, assuming angular momentum and parity conservation.

For transitions to discrete final states of spin J, additional information about the scattering amplitude can be obtained by studying the polarization of the recoil nucleus. This can be achieved through measurements of the angular correlation between the scattered proton and the particle(s) emitted in the nuclear deexcitation, as in reactions of the type $(\vec{p},p'\gamma)$. Such measurements, in which the polarizations of the outgoing proton and photon are not detected, are now technically quite feasible. Of particular interest are studies involving fairly simple (i.e., low angular momentum) spin sequences, such as a $0^+\rightarrow 1^+$ proton-induced transition, followed by deexcitation via photon emission to the 0^+ ground state. Counting arguments show that the scattering amplitude for this process can be characterized by a relatively small number of terms. For this particular case, it has in fact been recently shown [3–5] that certain $(\vec{p},p'\gamma)$ measurements, when combined with complete sets of $(\vec{p},\vec{p}')$ observables as discussed above, provide sufficient information to specify completely the scattering amplitude for the transition.

There has long been considerable interest, on both experimental and theoretical fronts, in $(p,p'\gamma)$ measurements for $0^+\rightarrow J^\pi$ transitions. It has been shown in the general case [6] that, for any $0^+\rightarrow J^\pi$ (p,p') transition, followed by γ decay to the ground state, certain combinations of $(\vec{p},\vec{p}')$, $(\vec{p},\vec{p}'\gamma)$, and $(p,p'\vec{\gamma})$ observables provide enough information to allow for a complete determination of the scattering amplitude. Some of these measurements, however, are experimentally quite difficult, since they involve detection of the circular polarization of the emitted γ rays. For the more specific case of a $0^+\rightarrow 1^+$ transition, though, recent theoretical work has shown [3–5] that the full scattering amplitude can be determined through measurements of any of several different combinations of $(\vec{p},p'\gamma)$ observables, combined with an appropriate set of $(\vec{p},\vec{p}')$ observables. Because the difficult photon polarization measurements need not be performed for

*Present address: Laboratory for Nuclear Science, Massachusetts Institute of Technology, Cambridge, MA 02139.
†Present address: Pacific Northwest Laboratories, Battelle Memorial Institute, Richland, WA 99352.
‡Present address: Department of Physics, Campbellsville College, Campbellsville, KY 42718.

this particular spin sequence, experimental study of these reactions seemed promising.

The isovector 1^+ state in ^{12}C at 15.11 MeV is an excellent candidate for an investigation of this sort, due to several important factors. Its large branching ratio to the ground state ($\Gamma_0/\Gamma \sim 0.92$) [7] makes it possible to acquire high yields, and therefore make statistically meaningful measurements, in a relatively short amount of time. The excitation energy is quite high, thereby making the events of interest easy to identify in a photon energy spectrum. Finally, this state has been extensively investigated in many previous studies, which have employed a wide variety of probes operating under many kinematic conditions.

Understanding the behavior of the 15.11 MeV state in ^{12}C has therefore often been viewed as a critical test of our models of the nucleon-nucleus (NA) interaction. Early measurements of $d\sigma/d\Omega$ and A_y for this state [8,9], taken at 200 MeV over a broad range of momentum transfer q, provided some of the first detailed comparisons between inelastic scattering data and predictions from then state-of-the-art distorted wave impulse approximation (DWIA) calculations at intermediate energies. These calculations, which had described data measured for this same transition at lower energies reasonably well [8], were found to disagree significantly with the data taken at this higher energy and at larger momentum transfers. It was argued at the time [9] that the deterioration of the agreement between these calculations and the new 200 MeV data might be due primarily to changes in the effective NN interaction encountered at higher energies.

To test these ideas more rigorously, one must be able to isolate specific pieces of both the effective interaction and the nuclear structure. This requires, as will be shown below, that one measure observables other than just cross sections and analyzing powers. In particular, the difference between the induced polarization and reaction analyzing power, $P-A_y$, was recognized early on as a combination of observables which, for inelastic transitions, should be especially sensitive to the tensor piece of the effective NN interaction, as well as its nonlocal or exchange nature. A measurement of $P-A_y$ at 150 MeV [10] for the 15.11 MeV state in ^{12}C showed this indeed to be the case, as did a later measurement of this observable at 400 MeV for the same state [11]. In both cases, inclusion of the tensor-exchange piece of the interaction was crucial in order for the DWIA calculations to agree with the measured values. This prompted detailed theoretical investigations by Love and Comfort [12] who were able to show, in a nonrelativistic framework, that isovector, $0^+ \rightarrow 1^+$ transitions were sensitive to the coupling of the nucleon spin to the bound nucleon current, and that understanding how these couplings arise through exchange was important for interpretation of the $P-A_y$ data for these transitions. It was later shown, in relativistic treatments of proton-nucleus scattering [13,14], that these same nuclear current terms appear more naturally in a relativistic formalism through the linear couplings between the upper and lower components of the bound nucleon wave function.

By extending these ideas to other observables, several groups [15,16] have independently shown that, in a plane-wave impulse approximation (PWIA), certain combinations of $(\vec{p},\vec{p}')$ spin-transfer observables show particular sensitivity to specific pieces of the effective nucleon-nucleon interaction and to various nuclear response functions. Thus, by forming these different combinations of observables, one can maximize sensitivity to different pieces of the interaction and/or nuclear structure. To construct these combinations, complete sets of $(\vec{p},\vec{p}')$ spin-transfer coefficients must be measured. This was first accomplished for the 15.11 MeV state in ^{12}C at an incident beam energy of 500 MeV at LAMPF [17] and later for this same state (and also for the isoscalar 1^+ state at 12.71 MeV) in a series of experiments carried out at IUCF [18,19] at 200 MeV. The data from LAMPF, although of poor statistical quality (typical uncertainties were ± 0.2), tended to agree at lower momentum transfers with DWIA calculations that used a free NN interaction. There were also suggestions [17] that, at least for some observables, relativistic impulse approximation calculations which did *not* explicitly include exchange contributions were able to reproduce the data better than similar calculations to which exchange effects had been added. The data from IUCF, on the other hand, were of sufficiently high statistical quality (uncertainties ranged from 0.02 to 0.06 in this momentum transfer range) that one could discriminate, in principle, between different models used to describe the NN interaction. However, there was limited coverage of momentum transfer in these data; complete sets of $(\vec{p},\vec{p}')$ observables were taken at only two proton scattering angles. Thus it was difficult to draw firm conclusions regarding details of the effective NN interaction from these early spin-transfer studies.

To further our understanding of proton-nucleus scattering at intermediate energies, it was evident that measurements of observables for more exclusive nuclear processes were necessary. Given the properties of the 15.11 MeV state and its γ decay as discussed above, the $(p,p'\gamma)$ reaction channel for this transition seemed relatively amenable to experimental study. The first measurements of $(p,p'\gamma)$ observables at intermediate energies for the 15.11 MeV state in ^{12}C were performed by Hicks *et al.* [20] at 400 MeV. In this work, the (p,p') singles and $(p,p'\gamma)$ coincident differential cross sections were measured for photons emitted either in or perpendicular to the scattering plane. These studies suggested [20] that calculations carried out in a relativistic formalism described the coincident observables better than those derived in a nonrelativistic framework. These coincident observables were quickly shown [3] to be sensitive to the composite spin-convection current amplitudes $\langle \boldsymbol{\sigma}\cdot\mathbf{j} \rangle$ and $\langle \boldsymbol{\sigma}\times\mathbf{j} \rangle$, which arise naturally in a relativistic formalism, but appear in nonrelativistic treatments of proton-nucleus scattering only through explicit treatment of exchange processes.

There has also been a report from Kovash [21] in which the $(\vec{p},p'\gamma)$ reaction was used at 150 MeV to determine the "singles" quantity $P-A_y$ for the 15.11 MeV state in ^{12}C. This required use of a polarized incident proton beam and detection of the outgoing photon along the normal to the reaction plane. This illustrates nicely how certain $(\vec{p},p'\gamma)$ observables can provide the same information that is contained in the more familiar $(\vec{p},\vec{p}')$ observables, a point that will be demonstrated more explicitly in the following section. More recently, coincident polarization asymmetries were measured for the 15.11 MeV state using the $(\vec{p},p'\gamma)$ reaction at 318 MeV [22], involving incident proton beam polarizations oriented along the normal, sideways, and lon-

gitudinal directions. In this experiment, however, the proton yields that were obtained represent integrals over the entire angular range studied ($\theta_p^{\text{c.m.}}=3.7°-12.4°$), and significant systematic errors were noted in extracting the true p-γ coincidences. The asymmetries determined in this work were nearly always consistent with zero and differed from the calculations to which the data were compared at all photon angles.

In each of the $(\vec{p},p'\gamma)$ studies discussed above, however, the needed complementary set of $(\vec{p},\vec{p}')$ spin-transfer observables were not measured. In this work, we have carried out *simultaneous* measurements of $(\vec{p},\vec{p}')$ and $(\vec{p},p'\gamma)$ observables for the 1^+, $T=1$ state at 15.11 MeV in ^{12}C at a bombarding energy of 200 MeV, using proton beams with their polarization vector oriented either normal to or lying in the reaction plane. Because of the large number of observables we were able to measure, we have obtained (as will be shown below) excellent internal consistency checks on our data, as well as enough information, in principle, to allow for a complete determination of the scattering amplitude for this transition. This latter procedure will be discussed in detail in another paper. In this paper, we present the data for all of our singles and coincident observables, and compare them with recent calculations [23] performed in both relativistic and nonrelativistic formalisms. This large data set necessarily imposes severe constraints on theoretical models that aspire to describe all of the observables.

This paper will be organized in the following way. In Sec. II we present the formalism adopted (from Ref. [3]) for analysis of the data and, where possible, indicate the physical content of the theory to which various observables are expected to be sensitive. In Sec. III, we describe our experimental apparatus, including both proton and photon detection systems, as well as the experimental procedures followed during data acquisition. We provide details of the data analysis in Sec. IV and demonstrate some of the internal consistency contained in the data set. In Sec. V the final values of all of our observables are presented and compared to the predictions of calculations that have been performed in either relativistic or nonrelativistic frameworks. Our most significant results and conclusions are summarized in Sec. VI.

II. FORMALISM

We will work in the orthogonal coordinate system

$$\mathbf{n}\equiv\mathbf{p}\times\mathbf{p}', \quad \mathbf{K}\equiv\mathbf{p}+\mathbf{p}', \quad \mathbf{q}\equiv\mathbf{n}\times\mathbf{K}, \tag{1}$$

where $\mathbf{p}$ ($\mathbf{p}'$) is the incident (outgoing) proton momentum, $\mathbf{n}$ is a vector directed perpendicular to the scattering plane, $\mathbf{K}$ is along the direction of the average proton momentum, and, in the limit of zero Q value for the reaction, $\mathbf{q}$ would point in the direction of momentum transfer $\mathbf{p}'-\mathbf{p}$. In this frame, the most general form of the scattering amplitude for a $0^+\rightarrow1^+$ transition, assuming only angular momentum and parity conservation, can be written [3]

$$\begin{aligned}\hat{T}^p(\mathbf{p},\mathbf{p}')=&A_{n0}(\hat{\boldsymbol{\Sigma}}\cdot\hat{\mathbf{n}})+A_{nn}(\hat{\boldsymbol{\Sigma}}\cdot\hat{\mathbf{n}})(\boldsymbol{\sigma}\cdot\hat{\mathbf{n}})\\&+A_{KK}(\hat{\boldsymbol{\Sigma}}\cdot\hat{\mathbf{K}})(\boldsymbol{\sigma}\cdot\hat{\mathbf{K}})+A_{Kq}(\hat{\boldsymbol{\Sigma}}\cdot\hat{\mathbf{K}})(\boldsymbol{\sigma}\cdot\hat{\mathbf{q}})\\&+A_{qK}(\hat{\boldsymbol{\Sigma}}\cdot\hat{\mathbf{q}})(\boldsymbol{\sigma}\cdot\hat{\mathbf{K}})+A_{qq}(\hat{\boldsymbol{\Sigma}}\cdot\hat{\mathbf{q}})(\boldsymbol{\sigma}\cdot\hat{\mathbf{q}}),\end{aligned} \tag{2}$$

where

$$\hat{\Sigma}_M\equiv|1^+M\rangle\langle0^+| \tag{3}$$

is the polarization operator for exciting the 0^+ ground state nucleus to a state with $J^\pi=1^+$ and magnetic substate M, $\vec{\sigma}$ are the Pauli spin operators for the projectile, and the $A_{i\mu}$'s are scalar functions of energy and momentum transfer. The subscripts i and μ for the individual amplitudes $A_{i\mu}$ represent the polarization components of the recoil 1^+ nucleus and scattered proton, respectively. Because there are only 6 allowed complex amplitudes, it is seen that a total of 11 pieces of information (after eliminating one overall, unphysical phase) are required in order to specify completely the scattering amplitude for this transition.

If the final polarization of the nuclear state is undetected, the spin observables can be expressed as

$$\begin{aligned}\frac{d\sigma}{d\Omega_p}&=\sum_{ij\mu}A_{i\mu}A^*_{j\mu}\delta_{ij},\\\frac{d\sigma}{d\Omega_p}D_{\alpha\beta}&=\sum_{ij\mu\nu}A_{i\mu}A^*_{j\nu}\delta_{ij}\frac{1}{2}\,\mathrm{Tr}[\sigma_\alpha\sigma_\mu\sigma_\beta\sigma_\nu],\end{aligned} \tag{4}$$

where $\alpha,\beta=0,n,K,q$. Using a scattering amplitude constrained by angular momentum and parity conservation [Eq. (2)] and carrying through the Pauli algebra, it can be shown that only 8 of the 16 possible singles $(\vec{p},\vec{p}')$ spin observables ($D_{\alpha\beta}$) are nonzero. Because 11 independent quantities must be measured to determine the scattering amplitude, one sees that there is information contained in the scattering amplitude which is not accessible in $(\vec{p},\vec{p}')$ singles measurements. In particular, the presence in Eq. (4) of the Kronecker δ_{ij} in the definition of the singles observables makes it impossible to determine the relative phases between individual amplitudes that correspond to recoil nuclear polarizations oriented in orthogonal directions.

If one makes the assumption that the $(p,p'\gamma)$ reaction is a strictly two-step process, i.e., that the transition amplitude can be written as the product of the strong and electromagnetic transition amplitudes, then one can show [3] that all of the coincident $(p,p'\gamma)$ observables can be written in terms of the singles (p,p') scattering amplitudes, $A_{i\mu}$, and the γ-ray branching ratio to the ground state, R. In complete analogy with the singles observables, the coincident spin-transfer observables for this transition can be written in the form [3]

$$\begin{aligned}\frac{d^2\sigma}{d\Omega_p d\Omega_\gamma}(\hat{\mathbf{k}})&=\frac{3R}{8\pi}\sum_{ij\mu}A_{i\mu}A^*_{j\mu}t_{ij}(\hat{\mathbf{k}}),\\\frac{d^2\sigma}{d\Omega_p d\Omega_\gamma}(\hat{\mathbf{k}})D_{\alpha\beta}(\hat{\mathbf{k}})&=\sum_{ij\mu\nu}A_{i\mu}A^*_{j\nu}t_{ij}(\hat{\mathbf{k}})\frac{1}{2}\,\mathrm{Tr}[\sigma_\alpha\sigma_\mu\sigma_\beta\sigma_\nu],\end{aligned} \tag{5}$$

where $\hat{\mathbf{k}}$ is the momentum direction of the emitted photon and the photon polarization tensor is given by

$$t_{ij}(\hat{\mathbf{k}})\equiv\delta_{ij}-(\hat{\mathbf{k}}\cdot\hat{\mathbf{e}}_i)(\hat{\mathbf{k}}\cdot\hat{\mathbf{e}}_j), \tag{6}$$

with $\hat{\mathbf{e}}_i$ and $\hat{\mathbf{e}}_j$ unit vectors from the $(\hat{\mathbf{n}},\hat{\mathbf{K}},\hat{\mathbf{q}})$ coordinate system defined in Eq. (1). It is important to emphasize that the

coincident observables are written in terms of bilinear products of the *same* $A_{i\mu}$'s as are the singles observables. The crucial difference between these two sets of equations is the presence of $t_{ij}(\hat{\mathbf{k}})$ in the definition of the coincident observables, replacing the δ_{ij} for the singles observables. Thus we see that the $(\vec{p},\vec{p}'\gamma)$ observables are sensitive to the relative phases between amplitudes for nuclear polarization projections in different directions, provided that the γ ray emitted has momentum components along both $\hat{\mathbf{e}}_i$ and $\hat{\mathbf{e}}_j$. Examples of these are found in the sideways and longitudinal analyzing powers $D_{0S}(\hat{\mathbf{k}})$ and $D_{0L}(\hat{\mathbf{k}})$, which vanish identically in $(\vec{p},p')$ measurements. These observables are related to the corresponding center-of-mass asymmetries $D_{0q}(\hat{\mathbf{k}})$ and $D_{0K}(\hat{\mathbf{k}})$ via

$$\begin{pmatrix} D_{0L}(\hat{\mathbf{k}}) \\ D_{0S}(\hat{\mathbf{k}}) \end{pmatrix} = \begin{pmatrix} \cos\theta_{pK} & -\sin\theta_{pK} \\ \sin\theta_{pK} & \cos\theta_{pK} \end{pmatrix} \begin{pmatrix} D_{0K}(\hat{\mathbf{k}}) \\ D_{0q}(\hat{\mathbf{k}}) \end{pmatrix}, \quad (7)$$

where θ_{pK} is the angle between the beam direction $\mathbf{p}$ and the average momentum $\mathbf{K}$. Through explicit expansion of Eq. (5), $D_{0K}(\hat{\mathbf{k}})$ and $D_{0q}(\hat{\mathbf{k}})$ can be shown to have the form

$$\frac{8\pi}{3R}\frac{d^2\sigma}{d\Omega_p d\Omega_\gamma}(\hat{\mathbf{k}})D_{0K}(\hat{\mathbf{k}}) = 2[\mathrm{Re}(A_{n0}A^*_{Kk}) - \mathrm{Im}(A_{nn}A^*_{Kq})]t_{nK}(\hat{\mathbf{k}}) + 2[\mathrm{Re}(A_{n0}A^*_{qK}) - \mathrm{Im}(A_{nn}A^*_{qq})]t_{nq}(\hat{\mathbf{k}}), \quad (8)$$

$$\frac{8\pi}{3R}\frac{d^2\sigma}{d\Omega_p d\Omega_\gamma}(\hat{\mathbf{k}})D_{0q}(\hat{\mathbf{k}}) = 2[\mathrm{Re}(A_{n0}A^*_{Kq}) + \mathrm{Im}(A_{nn}A^*_{KK})]t_{nK}(\hat{\mathbf{k}}) + 2[\mathrm{Re}(A_{n0}A^*_{qq}) + \mathrm{Im}(A_{nn}A^*_{qK})]t_{nq}(\hat{\mathbf{k}}). \quad (9)$$

In general, the scattering amplitude for (p,p') transitions can be divided more intuitively into two parts: terms which couple the proton spin to unit vectors that lie in the scattering plane, and those terms in which the proton spin couples to the unit vector normal to the reaction plane. Inspection of Eqs. (8) and (9) shows that certain $(\vec{p},p'\gamma)$ observables can access the relative phases between these two sets of terms, whereas singles $(\vec{p},\vec{p}')$ measurements cannot. Further, the form of the photon polarization tensor $t_{ij}(\hat{\mathbf{k}})$ implies that these terms can *only* be accessed if the coincident γ rays are detected at some angle that lies out of the scattering plane, yet is not normal to it.

Through measurements of $(\vec{p},p'\gamma)$ observables, one can also gain access to information about the scattering amplitude which can be obtained from singles $(\vec{p},\vec{p}')$ measurements only by detecting the polarization of the outgoing proton (using double-scattering techniques). Because of the transverse nature of a photon, when a coincident γ ray is emitted along the normal to the scattering plane, the photon necessarily has helicity components which lie in the scattering plane. Because the helicity components of the photon must couple to the polarization vector of the excited target nucleus for $1^+\rightarrow 0^+$ decays [3], the only terms in the transition amplitude which can contribute are those in which the polarization operator for the excited nucleus has components that lie in the scattering plane, i.e., along $\hat{\mathbf{K}}$ or $\hat{\mathbf{q}}$. Inspection of the structure of $\hat{T}^p$ [see Eq. (2)] shows that in this case the only polarization operators for the projectile which contribute are those involving a projectile spin flip with respect to $\hat{\mathbf{n}}$. These coincident yield observables are therefore sensitive to the *same* information carried by the normal $(\hat{\mathbf{n}})$ component $(\vec{p},\vec{p}')$ spin-transfer observables P, A_y, and $D_{N'N}$. Because we measured sets of $(\vec{p},\vec{p}')$ and $(\vec{p},p'\gamma)$ observables simultaneously and detected coincident photons along the $\hat{\mathbf{n}}$ direction, we were able to perform several of the valuable internal consistency checks on the quality of our data alluded to earlier.

III. EXPERIMENTAL APPARATUS AND TECHNIQUES

The experiment reported here was carried out at the Indiana University Cyclotron Facility with a 199.8 MeV polarized proton beam. The beam energy was determined by closing down slits around the beam just upstream and downstream from a calibrated 45° analysis magnet and, independently, with a pair of beam time-of-flight pickoff units located in a straight section of beam line upstream of this magnet. The proton beam was produced using a standard atomic beam polarized ion source [24] and accelerated through two cyclotrons, during which time the polarization vector of the beam remains pointing very close to vertical.

For measurements of the normal-component $(\vec{p},\vec{p}')$ spin-transfer observables and coincident $(\vec{p},p'\gamma)$ yields and asymmetries, the beam was transported directly to the experimental area. Some of the observables measured, however, required that the polarization vector of the incident beam be first rotated to lie in the reaction plane. This was achieved through the use of two superconducting solenoids, with magnetic fields aligned parallel to the beam momentum, that were positioned upstream and downstream of the 45° analysis magnet. At this beam energy, the precession of the proton's spin (about the vertical axis) induced by this dipole (97.9°) is sufficiently close to 90° that we could orient the final proton polarization vector to point in almost any direction desired through the appropriate adjustment of the two solenoid currents. High-energy in-beam (i.e., transmission) $p+d$ polarimeters [25] continuously monitored both the normal (vertical) and sideways polarization components of the beam. Because a polarimeter was positioned immediately downstream of each solenoid and because the spin precession angle in each solenoid was known, we could uniquely determine the proton polarization direction and magnitude everywhere in the high-energy beam lines, without any prior assumptions as to the polarization properties of the beam extracted from the cyclotrons. Typical values of the magnitude of the beam polarization determined for each incident orientation and at each proton scattering angle were $\langle P\rangle \approx 0.75\pm 0.01$. The proton polarization direction was also reversed by 180° (using RF transitions in the ion source) every 20 s during this work.

Because $0^+\rightarrow 1^+$ transitions are of unnatural parity, they occur predominantly through an orbital angular momentum change $\Delta L=0$. As such, they are expected to be very forward peaked in the laboratory frame at intermediate energies, with cross sections that decrease rapidly with increasing proton scattering angle. This behavior has been verified experimen-

tally [8] for the 15.11 MeV state in ^{12}C. To obtain appreciable yields and thereby make statistically meaningful measurements in this work, it was therefore necessary to detect the inelastically scattered protons at small laboratory angles. Moreover, because the photon detectors were positioned very close to the target (to maximize the coincident solid angle), it was essential that the unscattered beam be deposited in a well-shielded beam dump far downstream from the target; this would minimize the background seen by the photon detectors, thus allowing for cleaner identification of the true coincident γ rays. To meet both of these requirements, during data acquisition we utilized a septum magnet [26] that had been recently installed on the IUCF K600 spectrometer, which we describe below.

The K600 magnetic spectrometer system is a quadrupole-dipole-dipole configuration [27] which bends the scattered protons in the horizontal reaction plane. In previous measurements of spin observables at small scattering angles ($\theta_p \sim 7°$), the unscattered beam was deposited in a compact Faraday cup mounted inside the target chamber [19]. In this configuration, even relatively small amounts of beam (~2 nA) incident on the K600 target can generate large amounts of room background. For the present experiment, the use of this "internal" Faraday cup would have resulted in copious fluxes of charged particles, neutrons, and photons, originating from a source almost as close to the photon detectors as the target itself, thereby rendering the identification of the true coincident γ rays virtually impossible. With the use of the septum magnet (essentially a small dipole mounted between the target chamber and the entrance quadrupole of the K600 magnet system), protons scattered at laboratory angles as small as $\theta_p = 5°$ were bent into the acceptance of the spectrometer (collimated to be $\Delta\Omega = 0.445$ msr), while the unscattered beam was allowed to pass to a well-shielded beam dump located ~7 m downstream from the target. In this mode of operation, we were able to detect cleanly the γ rays of interest. The coincident inelastically scattered protons that entered the spectrometer were momentum analyzed using the focal plane wire chambers and scintillators, and their transverse (vertical and sideways) polarization components were measured in the associated focal plane polarimeter (FPP) [28].

The coincident γ rays were detected in four large arrays of BaF_2 [29], provided by the Oak Ridge National Laboratory collaboration. BaF_2 was a logical choice for coincident γ detection in the K600 environment, primarily due to its dual component response. These crystals have the advantage of both excellent timing characteristics (due to a fast response component, with $\lambda \sim 200$ nm) and the ability to maintain energy resolution (this from a slow component, with $\lambda \sim 310$ nm) comparable to more conventional γ detectors, such as thallium-doped NaI, which have much poorer timing characteristics. Shown in Fig. 1 is one of the four close-packed 19-detector bundles, or 19-packs, used for these measurements. Each of the 19 BaF_2 crystals in each pack is hexagonal in cross section, 6.5 cm across and 20 cm deep, which is sufficiently thick to stop a normally incident 15 MeV γ ray with a conversion efficiency well above 99%. Associated with each crystal is an individual photomultiplier tube, with a quartz window to the photocathode (to pass the fast light), and a highly stabilized base.

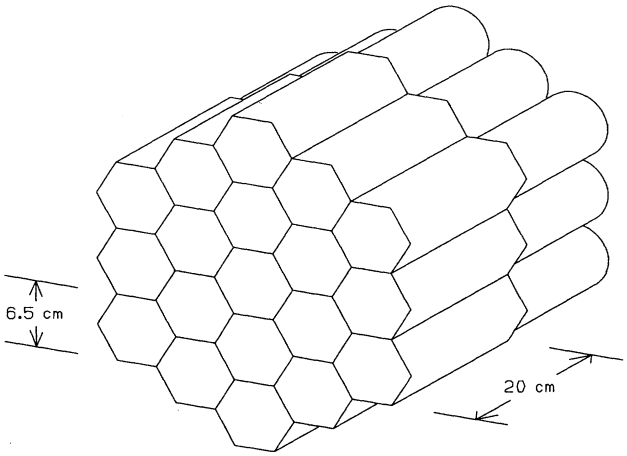

FIG. 1. Schematic of a close-packed 19-detector bundle of BaF_2 detectors. The attached cylinders represent phototube and base assemblies.

In order to minimize the attenuation of the γ-ray flux of interest and to ensure that this attenuation was nearly independent of θ_γ, a special thin-walled scattering chamber, compatible with all of the septum magnet mode hardware, was installed for these measurements. The scattering chamber was cylindrical, with the symmetry axis oriented perpendicular to the scattering plane. The aluminum chamber had 6.4 mm thick walls and an outer diameter of 25.4 cm. The upper lid of the chamber was also 6.4 mm thick, to ensure that the photon flux which entered the BaF_2 array positioned directly above the target experienced the same attenuation as did the photons emitted in the scattering plane. With this choice of geometry for the scattering chamber and for the positions of the BaF_2 arrays (discussed below), the attenuation of the emitted γ-ray flux in the chamber walls was nearly independent of photon angle and was estimated to be approximately 4% for $E_\gamma = 15.11$ MeV.

There were three different types of events which generated valid trigger signals in the acquisition logic: valid K600 focal plane events [prescaled, typically by 10, and used for $(\vec{p},p')$ cross section and analyzing power measurements]; a logic signal which indicated that potentially useful information was available in the FPP detectors [for $(\vec{p},\vec{p}')$ singles spin-transfer measurements]; and a logic signal generated by a timing coincidence (~200 ns overlap) between the K600 focal plane signal and a 76-fold fast OR of high-threshold discriminators on the photon detectors (set in hardware at 200 mV, corresponding approximately to a 2 MeV γ ray), indicating that a relatively large amount of energy had been deposited in at least one of the BaF_2 crystals [for measurements of $(\vec{p},p'\gamma)$ observables]. For this last type of event, three signals were read out by CAMAC for each BaF_2 detector that exceeded a low-threshold discriminator (set at 50 mV, corresponding approximately to a 500 keV γ ray): fast timing information, relative to the K600 focal plane scintillator; a wide-gate (1.5 μs) pulse height integral, for high resolution over the energy range of interest; and a short-gate (50 ns) pulse height integral, whose amplitude is dominated

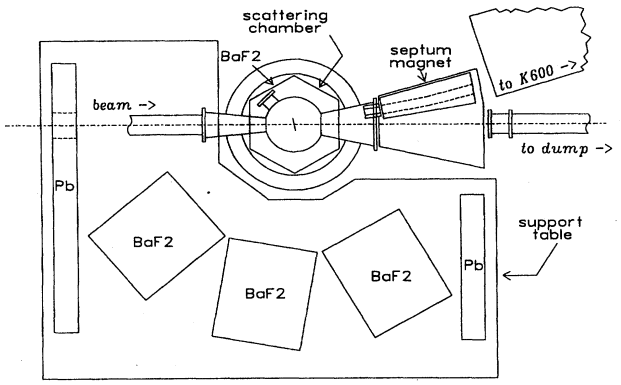

FIG. 2. Schematic diagram showing the position of the four BaF_2 arrays relative to the thin-walled scattering chamber, septum magnet (and associated hardware), and K600 entrance quadrupole.

by the fast (ultraviolet) component of the scintillator response. These signals were used to provide tight time correlation with the proton arrival time at the K600 focal plane scintillator and pulse-shape discrimination of photons against both charged particles and neutrons.

Because it was crucial for identification of the true coincident γ rays that this information be of high quality, we were limited in the singles rates we could tolerate in the BaF_2 crystals, which ultimately resulted in limiting the rate at which we could acquire data. Typical running conditions for the four proton scattering angles studied ($\theta_p^{\text{c.m.}}=5.5°$, 8.8°, 12.1°, and 16.5°) were 2 nA of beam incident on a 93.8 mg/cm^2 $^{\text{nat}}$C target [this thickness was chosen to maximize the ratio of "real" events relative to "accidental" events, as defined below, for the $(\vec{p},p'\gamma)$ events]. Under these conditions, the total low-threshold rate in all 76 BaF_2 detectors was ~20 MHz, with each crystal having a singles rate of ~250 kHz. This was approximately the limit beyond which the BaF_2 detectors would not perform well enough to carry out these measurements.

For the two different modes of running, i.e., incident beam polarizations oriented either normal to or lying in the scattering plane, the BaF_2 arrays were also positioned differently. When the beam polarization was vertical (normal to the reaction plane), three BaF_2 arrays were positioned to lie in the scattering plane, at laboratory angles of $\theta_\gamma^{\text{lab}}=60°$, 100°, and 140° on beam right, with the front face of each array 56 cm from the center of the target. A schematic diagram of our equipment in this configuration is shown in Fig. 2, illustrating the position of the BaF_2 arrays relative to the thin-walled scattering chamber, septum magnet, and K600 entrance quadrupole. Because of the large charged-particle flux emitted at forward angles from the thick carbon target, we found it necessary to cover the front face of the most forward BaF_2 array with 3.6 cm of aluminum, which was sufficient to stop protons of up to ~100 MeV. Details of the required attenuation correction introduced by the addition of this aluminum absorber will be discussed in the following section. A fourth BaF_2 array was positioned directly above the target (for both modes of running), with its front face 52 cm away from the center of the target; the outline of this hexagonal array can also be seen in Fig. 2.

With this combination of vertical beam polarization and in-plane photon detector placement, we measured the singles observables $d\sigma/d\Omega$, A_y, P, and $D_{N'N}$, and simultaneously measured the coincident double-differential cross section $d^2\sigma(\theta_\gamma)/d\Omega_p d\Omega_\gamma$ and normal-component polarization asymmetry $A_y(\theta_\gamma)$ as a function of photon angle in the scattering plane. We also measured a coincident cross section and polarization asymmetry using the BaF_2 array placed directly above the target. As mentioned earlier, coincidence observables in which the photon is emitted along the normal to the reaction plane are sensitive to the same information as is carried by the normal-component $(\vec{p},\vec{p}')$ spin-transfer observables. The resulting internal consistency contained in our data will be presented later.

For the second set of observables, i.e., those which involve incident proton beam polarizations that lie *in* the reaction plane, we chose to make measurements with three different orientations of the incident proton polarization for each proton scattering angle, at in-plane laboratory angles of $\phi_p=53°$, 117°, and 169°. (ϕ_p is the angle of the proton polarization vector, measured with respect to the incident beam direction.) With these polarizations, we were able to determine two linear combinations of the four in-plane singles spin-transfer coefficients using the FPP,

$$\begin{aligned} D_\lambda &\equiv D_{L'L}\sin\alpha + D_{S'L}\cos\alpha, \\ D_\sigma &\equiv D_{L'S}\sin\alpha + D_{S'S}\cos\alpha, \end{aligned} \tag{10}$$

where α (≈264°) is the angle of (horizontal) spin precession experienced by the scattered proton flux in the dipole fields of the K600 spectrometer.

For the $(\vec{p},p'\gamma)$ coincident observables, the form taken by the longitudinal and sideways analyzing powers [Eqs. (8) and (9)] dictates that the maximal sensitivity to these observables is achieved if the photons are detected at an angle of 45° with respect to the $\hat{\mathbf{n}}$ direction, i.e., in a cone 45° *out* of the scattering plane. Thus, for this second data set, we supported three BaF_2 arrays at this angle above the scattering plane. In this case, the BaF_2 arrays were positioned on beam right at laboratory angles (projected into the scattering plane) of $\phi_\gamma^{\text{lab}}=41°$, 88.3°, and 140°. Because of space limitations, we were forced to place the arrays (center of the front face) at distances of 79, 66, and 66 cm from the target, respectively. In this configuration, the three BaF_2 arrays were used to map out the angular distributions of the coincident yield spin asymmetries, from which D_{0S} and D_{0L} can be determined. The use of three different incident beam polarization orientations (ϕ_p) allowed us to separate the sideways and longitudinal pieces, and also provided another internal consistency check, in that only two orientations were actually needed. This is because the polarization asymmetry mapped out in the 45° cone depends sinusoidally on both the incident proton spin orientation and the direction of the emitted photon; therefore, only four independent coefficients are needed to fully describe it.

In summary, we have measured 6 $(\vec{p},\vec{p}')$ singles observables ($d\sigma/d\Omega_p$, A_y, P, $D_{N'N}$, D_λ, and D_σ), along with 12 coincident observables: the $(\vec{p},p'\gamma)$ yields and normal-component asymmetries at in-plane angles of $\theta_\gamma^{\text{lab}}=60°$, 100°, and 140°, the coincident yield and normal-component

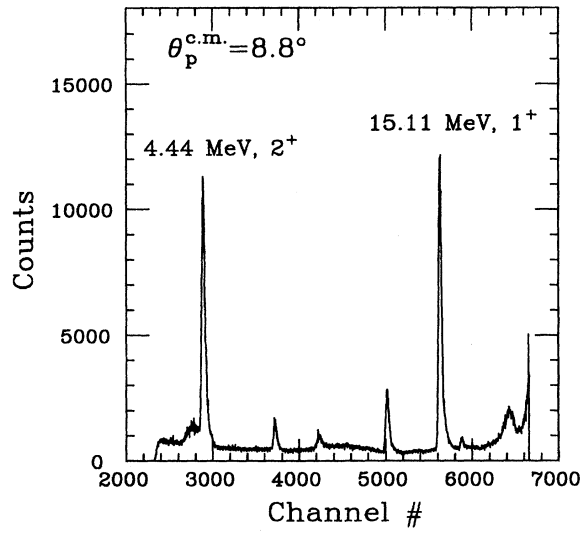

FIG. 3. $p+^{12}C$ excitation spectrum for $T_p=200$ MeV, $\theta_p^{c.m.}=8.8°$. Several prominent peaks are identified; other features are described in the text.

asymmetry when the photon was emitted along the normal to the reaction plane, and the four coefficients which describe the polarization yield asymmetry 45° out of the scattering plane when the beam polarization vector lies in the scattering plane. All of these observables have been measured for the 15.11 MeV, 1^+, $T=1$ state in ^{12}C at an incident beam energy of 200 MeV, at four proton scattering angles. For reasons that will be described in the following section, we were not able to obtain reliable estimates of the absolute cross section for this transition at all angles; nevertheless, at each angle we did obtain sufficient information to allow for a determination of the full scattering amplitude, details of which will be presented in a subsequent paper.

IV. DATA ANALYSIS

For each of the three types of events discussed in the previous section, the first step in our data reduction was to verify that we had a valid K600 focal plane event. This analysis depends principally on information obtained from two vertical drift chambers (VDC's) mounted in the spectrometer focal plane. The drift times from the wires in each chamber were converted to distances, and the trajectory of the proton as it passed through the chambers was calculated. Given that the proton position along the focal plane is (approximately) linearly related to its momentum, the resulting spectra represent the reaction yield as a function of the excitation energy of the target nucleus. Shown in Fig. 3 is one such spectrum, for the scattering of 199.8 MeV protons at $\theta_p^{c.m.}=8.8°$ from the 93.8 mg/cm^2 ^{nat}C target. Some of the better known excited states in ^{12}C are labeled. The small, somewhat broad peak that appears as a low-energy shoulder on the 4.4 MeV state is due to $p+p$ elastic scattering from hydrogen contamination in the target.

Some features of this spectrum (Fig. 3) are worthy of note. Perhaps most obvious is that, in the low excitation region, the elastic scattering peak is not present. Because the elastic scattering yield is so large at small scattering angles, this process would normally dominate the observed focal plane yield. The limitations this would impose on our data acquisition rates would have resulted in poor statistical quality for observables of the state of interest if the elastic yield had not been eliminated. To achieve this, a small plastic (NE102) "veto" scintillator was positioned in the focal plane detector stack near the region through which the elastically scattered protons would pass. A logic signal generated by this paddle was then used to veto the usual focal plane scintillator trigger. For similar reasons, the continuum yield at higher excitation energy was also eliminated, though in this case by disconnecting power to the preamplifier cards for the front VDC in this region of excitation.

Of more immediate significance to the present work, Fig. 3 shows that relatively large amounts of background exist underneath the 15.11 MeV peak in this spectrum. This background, dominated by a few very broad states in this excitation region [7] and the "slit-edge scattered" tail of the elastically scattered protons (from the inside walls of the septum magnet and its defining entrance collimator), would contaminate the peak yields for the 15.11 MeV state and would do so in a spin-dependent manner. Moreover, since this background is primarily due to natural parity transitions (while the 15.11 MeV state is of unnatural parity), the spin dependence of the background would be expected to be significantly different from that of the state of interest. To minimize the possibility of this contamination, we have developed a method [19] for incorporating the spin dependence of the background when subtracting these counts from the total peak yield. While this technique turned out to be very important for extracting yields for $(\vec{p},\vec{p}')$ singles events, imposing the coincident γ requirement was found to be an extremely efficient means of reducing this background, so that extracting peak yields for $(\vec{p},p'\gamma)$ events was generally much more straightforward.

The peak yields obtained from focal plane spectra, such as Fig. 3, when sorted on the incident beam spin state ("up" or "down"), could be used directly to extract the reaction differential cross section $d\sigma/d\Omega_p$ and analyzing power A_y, once corrections due to computer dead time, detector efficiencies, and integrated beam current differences between the two spin states had been incorporated. During off-line analysis, however, it was discovered that the electronic circuit which produced logic signals for the beam current integrator scaler was not operating properly during data acquisition, and would double fire for short, but irregular, periods of time. This made determination of precise values for $d\sigma/d\Omega_p$ impossible, and a detailed investigation of the possible effect of this equipment malfunction on extracting spin asymmetries was undertaken. By noting the typical time scale on which this problem occurred and comparing this to our "spin-flip" period of 20 s, it was determined that this problem would introduce false asymmetries much smaller than the statistical accuracy achieved for all observables and was therefore neglected in our analysis. Details of this investigation can be found in Ref. [30].

To determine $(\vec{p},\vec{p}')$ spin-transfer observables, spectra like Fig. 3 were generated after several FPP software condition tests had been applied to the data. While these tests have been documented at length elsewhere [19], we will give a

brief overview of this procedure. From the four multiwire proportional counters (MWPC's) located downstream from a 5 cm thick graphite analyzer, scattering vertex position and angle information were extracted on an event-by-event basis. If the vertex was determined to lie somewhere within the analyzer and at the correct vertical position, and if the magnitude of the scattering angle (in the analyzer) was determined to be greater than 5°, then a detailed analysis of the energy deposition in both the ΔE (6.4 mm thick) and E (7.6 cm thick) scintillator planes located just downstream of the four MWPC's was performed. If it was determined, via comparison of the measured versus expected energy losses in the two scintillator planes, that the proton had scattered elastically from a ^{12}C nucleus in the analyzer, then one of four focal plane spectra was incremented, sorted on both scattering direction in the analyzer (left or right for normal-component observables, up or down for in-plane component observables) and the spin state of the incident beam. Once the peak yields of interest were extracted, with background subtraction, from these four spectra, they were corrected for spin-dependent dead time, detector inefficiencies, and integrated beam current effects. These normalized yields, combined with knowledge of the incident beam polarization (from the high-energy in-beam polarimeters, discussed in the previous section) and the effective analyzing power of the FPP [31] (measured to be $A_{\rm FPP}=0.48\pm0.01$ at this energy), were used to determine the normal-component $(\vec{p},\vec{p}')$ singles observables A_y, P, and $D_{N'N}$ in a straightforward manner [19].

A bit more work was required to deduce the two linear combinations of the in-plane spin-transfer coefficients D_λ and D_σ that were defined earlier in Eq. (10). Because the up/down scattering yield asymmetry seen in the FPP can be due only to the sideways component of the proton polarization *at* the FPP (i.e., we have no experimental sensitivity to the longitudinal polarization of the scattered beam at the polarimeter), only one component of the in-plane polarization of the scattered beam can be measured at a time. By changing the in-plane orientation of the incident beam polarization, we can change the sideways polarization of the scattered beam at the FPP analyzer, but this does not provide sufficient information to allow us to isolate the four independent in-plane spin-transfer coefficients. This can be shown more explicitly by noting that the up/down asymmetry measured in the FPP can be related to the in-plane incident beam polarization vector (of magnitude P_T and orientation ϕ_p relative to the beam direction) via

$$\varepsilon_{\rm FPP}=P''_S A_{\rm FPP}=A_{\rm FPP}P_T(D_\lambda\cos\phi_p+D_\sigma\sin\phi_p). \quad (11)$$

In this equation, $P''_S=P'_L\sin\alpha+P'_S\cos\alpha$ is the sideways component of the scattered proton polarization at the FPP, i.e., after undergoing a rotation by α in the K600 magnet system. Equation (11) shows that by mapping out the dependence of the measured asymmetry, $\varepsilon_{\rm FPP}$, on the angle ϕ_p and fitting this asymmetry with a sinusoidal function, we can extract the two observables D_λ and D_σ. Since three incident polarization directions (ϕ_p) were used at each proton scattering angle, this also provides a consistency check on the quality of our measured FPP asymmetries (by noting the χ^2 for the fits) for the determination of these two observables. The

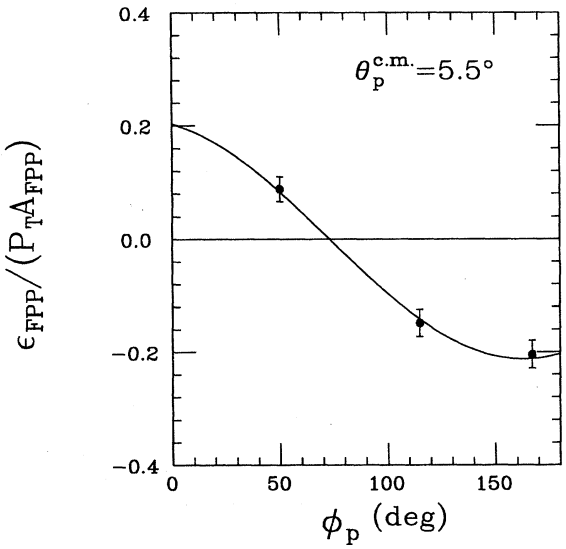

FIG. 4. Normalized asymmetry measured at the K600 FPP at $\theta_p^{\rm c.m.}=5.5°$, as a function of the in-plane beam polarization angle ϕ_p. Error bars represent statistical uncertainties only.

dependence of the measured FPP asymmetry on ϕ_p, normalized to P_T and $A_{\rm FPP}$, at a proton scattering angle of $\theta_p^{\rm c.m.}=5.5°$, is illustrated in Fig. 4.

In order to extract the $(\vec{p},p'\gamma)$ observables, the information contained in the BaF_2 detectors had to undergo significant processing. Before describing this analysis, we point out that the electronic gates sent to the integrating analog-to-digital converters (ADC's) used for the BaF_2 energy information were of order $\sim$1.5 μs wide, and the TDC modules used for BaF_2 timing information were set to ranges of order $\sim$200 ns, while the time structure of the incident beam dictated that "beam bursts" arrive at the K600 target approximately every 58 ns. It was therefore possible (and indeed crucial) that identical analyses be carried out on both "real" and "accidental" coincident events. "Real" events were those which contained the correct energy for the scattered proton and the correct energy and pulse shape for the γ ray, with the correct (coincident) time correlation between the two signals. "Accidental" events, on the other hand, contained the same information as the "reals" *except* that the γ-ray timing signal was generated during one of the beam bursts adjacent to the one in which the proton signal was generated. In this way, "accidental" events could be subtracted from the "real" events in a consistent manner. We also note that, in order to reduce the sensitivity of the extracted coincident yields and asymmetries to position within the 19-pack (background rates, for example, often varied significantly over the array), a separate but identical analysis was performed on each of the 76 BaF_2 crystals individually, and all solid-angle averaging was done appropriately at a later stage in the analysis.

After each of the BaF_2 detectors had been matched in time and energy response (done to the $\sim$10% level prior to data acquisition and improved with software gain and offset parameters during off-line replay), the first step in the BaF_2 analysis procedure was to discriminate between the γ rays of

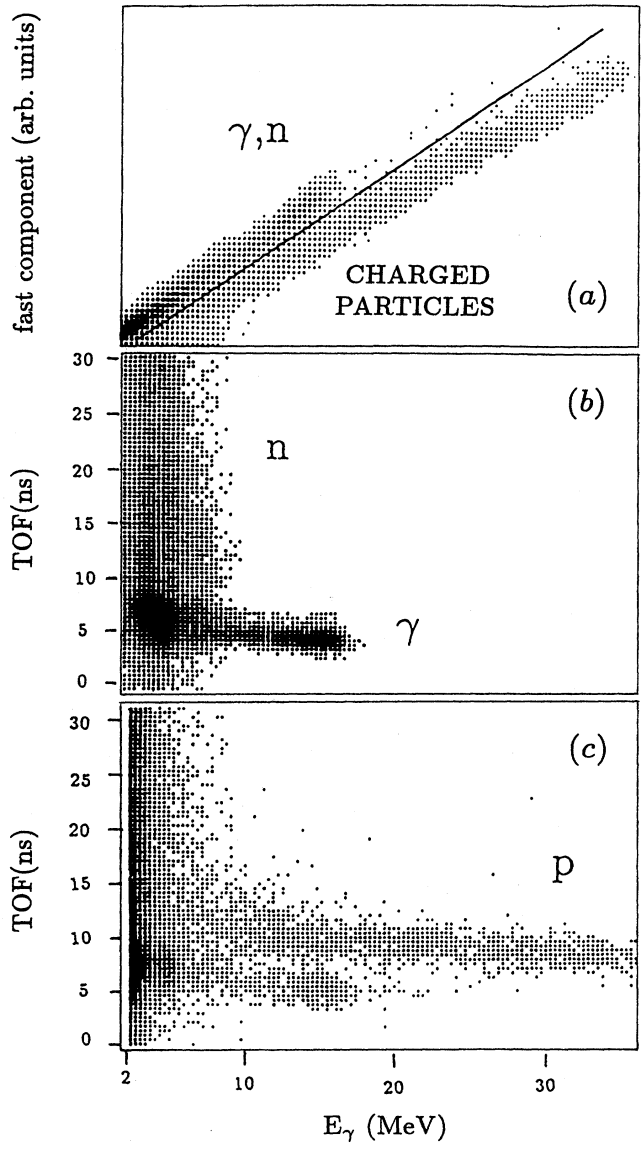

FIG. 5. (a) Correlation between the fast light component and the total light output for the 19 BaF_2 crystals located at $\theta_\gamma^{\text{lab}}=100°$, for $\theta_p^{\text{c.m.}}=8.8°$. The solid line is used to discriminate between charged particles (below line) and photons and neutrons (above line). (b) Distribution of the relative time of flight versus total γ-ray energy for photons and neutrons, as identified in plot (a). (c) Same as (b), but for charged particles.

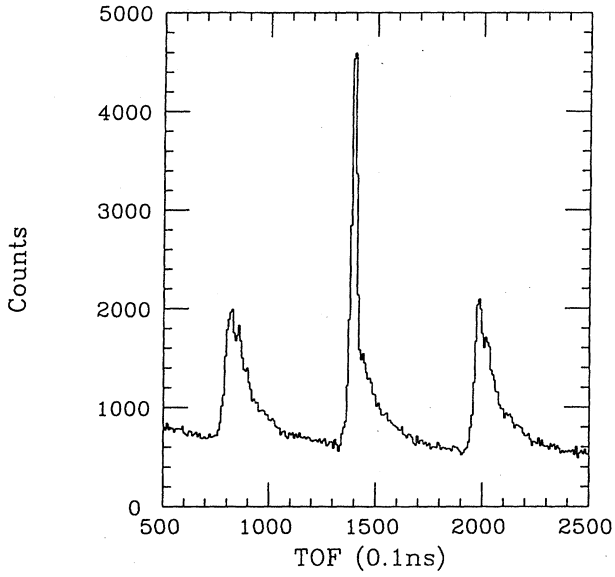

FIG. 6. Relative time-of-flight spectrum between proton arrival time at the K600 focal plane scintillator and photon arrival at the BaF_2 detectors at $\theta_\gamma^{\text{lab}}=100°$, for $\theta_p^{\text{c.m.}}=8.8°$. Pulse shape discrimination and corrections for differing proton flight times and electronic "walk" have been applied to the data, as described in the text.

interest and charged particles and neutrons. Shown in Fig. 5 are histograms which illustrate how this was accomplished. Following the method of Novotny *et al.* [32], we first used the correlation between the fast component of the scintillator response and the total light output to discriminate between neutral particles and charged particles (top figure). We then looked at the relative timing between the detection of the protons in the K600 focal plane and the neutral particles in the BaF_2 detectors, in order to separate the prompt γ rays from the time-uncorrelated neutrons (middle figure). A similar plot for the charged particle timing (bottom figure), in which distinct bands of protons and photons can be seen, indicates the high quality of this separation technique. The high-energy (E_γ>7 MeV) photons apparent in the bottom figure typically represented only ~2% of the total photon yield.

Having thus selected only events in which a real photon was detected, it was then necessary to identify those events in which the BaF_2 signal also had the correct time correlation and energy to be a possible coincident 15.11 MeV γ ray. After the relative time between the proton and photon signals was corrected to account for differing proton flight times through the spectrometer and for electronic "walk" in the leading-edge discriminators that were used to generate the BaF_2 logic signals, excellent timing information was obtained. A typical corrected time-of-flight (TOF) histogram is shown in Fig. 6, in which the "real" and "accidental" peaks are readily apparent, even before any photon or proton energy information has been incorporated into the event selection.

With appropriate gates now distinguishing between the "real" and "accidental" events, the final requirement of the BaF_2 information was that the energy signal be sufficiently large to serve as a potential 15.11 MeV candidate. Because, in most cases, not all of the 15 MeV of energy was deposited in a single crystal (recall that a separate analysis was performed on each individual detector), a low-energy software cut of only 7 MeV was imposed on each BaF_2 energy signal. A set of focal plane histograms (like Fig. 3) was then generated for every crystal, for both spin states of the beam and for both "real" and "accidental" beam bursts. With all of this information in hand, coincident $(\vec{p},p'\gamma)$ yields and

asymmetries could then be extracted for each individual crystal from the high-resolution [~70 keV full width at half maximum (FWHM)] focal plane spectra.

The final stage in our analysis involved converting these $(\vec{p},p'\gamma)$ yields into useful observables. With the incident beam polarization normal to the scattering plane, measurements of the normal-component coincident analyzing powers $A_y(\theta_\gamma)$ were made at in-plane photon angles of $\theta_\gamma^{\rm lab}=60°$, 100°, and 140°, while a fourth analyzing power $A_y(\hat{\mathbf{n}})$ was probed when the coincident photon was emitted along the normal to the scattering plane. With the incident beam polarization vector rotated *into* the scattering plane, measurements of the coincident yield asymmetries in a cone 45° out of plane were made for three different in-plane proton polarization orientations at three photon angles, thus providing a total (at each *proton* scattering angle) of nine measured asymmetries to determine four independent coefficients.

A bit of algebra shows that the spin-dependent coincident yield asymmetry measured in the cone 45° out of the reaction plane can be expressed in the form

$$\begin{aligned}\varepsilon_{\rm coin}(\phi_p,\phi_\gamma;\theta_{pK}) = &-\tfrac{1}{2}D_{0K}(nK)\cos(\phi_p-\theta_{pK})\cos(\phi_\gamma+\theta_{pK})+\tfrac{1}{2}D_{0K}(nq)\cos(\phi_p-\theta_{pK})\sin(\phi_\gamma+\theta_{pK})\\ &-\tfrac{1}{2}D_{0q}(nK)\sin(\phi_p-\theta_{pK})\cos(\phi_\gamma+\theta_{pK})+\tfrac{1}{2}D_{0q}(nq)\sin(\phi_p-\theta_{pK})\sin(\phi_\gamma+\theta_{pK}),\end{aligned} \tag{12}$$

where, as before, ϕ_p is the initial proton spin orientation in the scattering plane, ϕ_γ is the photon angle projected into the reaction plane on beam right, and θ_{pK} is the angle between the incident beam momentum **p** and the average momentum **K** [see Eq. (1)]. The coefficients $D_{0i}(nj)$ $(i,j=K,q)$ are the in-plane analyzing powers defined in Eqs. (8) and (9), where the indices i and j represent the polarization direction of the incident proton beam and the direction of the emitted photon, respectively. Because we have nine measurements to determine four coefficients, we can again test the internal consistency of our data through a χ^2 minimization procedure. In Fig. 7 the sinusoidal dependence of the measured asymmetry (normalized to the magnitude of the in-plane polarization) on the incident beam polarization direction ϕ_p is shown for data taken at a proton scattering angle of $\theta_p^{\rm c.m.}=5.5°$, for photons emitted at $\phi_\gamma=88.3°$. In Fig. 8 we illustrate a second sinusoidal dependence of this same asymmetry, in this case on the direction of the coincident γ ray, ϕ_γ, also for $\theta_p^{\rm c.m.}=5.5°$ and with ϕ_p fixed at 50.0°. For the examples shown here (the global fit of all nine asymmetries at $\theta_p^{\rm c.m.}=5.5°$) the χ^2 per degree of freedom was found to be 0.31.

Significantly more analysis was required to extract coincident $(\vec{p},p'\gamma)$ yields. As mentioned previously, because of the large charged-particle flux emitted from the target at forward angles, it was necessary to place 3.6 cm of aluminum in front of the most forward angle BaF_2 array. In order to correct for the resulting photon attenuation, a calibration technique had to be developed. For a portion of our run, we therefore replaced the $^{\rm nat}$C target with a 50.4 mg/cm^2 isotopically enriched ^{6}Li target and identified (through the same procedure outlined above, though now with a low-energy γ-ray threshold of only 2 MeV) the coincident photons re-

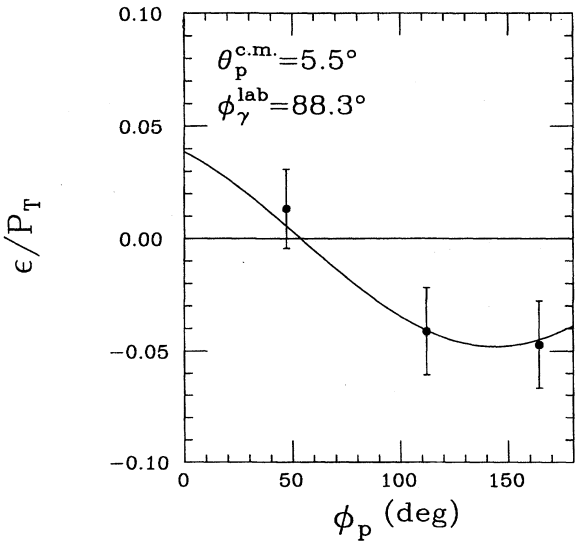

FIG. 7. $(\vec{p},p'\gamma)$ coincident yield asymmetry measured 45° out of plane at $\phi_\gamma^{\rm lab}=88.3°$, as a function of the in-plane beam polarization angle ϕ_p. The curve represents the global best fit asymmetry at $\theta_p^{\rm c.m.}=5.5°$. Error bars represent statistical uncertainties only.

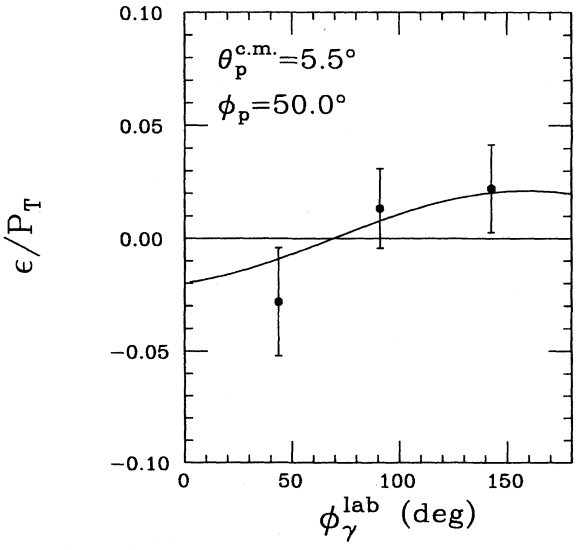

FIG. 8. $(\vec{p},p'\gamma)$ coincident yield asymmetry measured 45° out of plane when $\phi_p=50.0°$, as a function of the photon angle $\phi_\gamma^{\rm lab}$. The curve represents the global best fit asymmetry at $\theta_p^{\rm c.m.}=5.5°$. Error bars represent statistical uncertainties only.

sulting from deexcitation to the ground state of the 3.56 MeV 0^+ state in ^{6}Li. Because this is a 0^+ state, the decay γ rays are emitted isotropically. Further, because this state lies below particle threshold for this nucleus, the γ-decay branching ratio is 1, with almost 100% of the strength going to the ground state. Thus, by studying this reaction, we could directly determine the effective efficiency (i.e., the product of the coincident solid angle and the hardware and software efficiencies) of each BaF_2 crystal for 3.56 MeV γ rays. [Because of the recoil of the ^{6}Li nucleus, a small (typically 1%) correction for the Doppler effect was also applied to recover the isotropic distribution.] However, because both the intrinsic efficiency of BaF_2 and the attenuation of γ rays through aluminum are functions of the photon energy, it was necessary to employ GEANT [33] simulations to extrapolate these quantities reliably to the higher γ-ray energies appropriate for the transition studied in this work. We estimate that, with these corrections, all of our relative coincident yields (for different photon detector angles) are accurate at the 5% level. These corrections were not applied, though, to the coincident asymmetries, under the reasonable assumption that there was negligible spin dependence in either the BaF_2 efficiencies or the photon attenuation. (The individual BaF_2 low-threshold singles rates exhibited remarkably little spin dependence throughout the run.)

Because of the problem with the beam integrator scaler circuit mentioned earlier, it was not possible to extract absolute double-differential cross sections. We could, however, determine very precisely the ratio of the coincident cross section to the singles cross section $(d^2\sigma/d\Omega_p d\Omega_\gamma)/(d\sigma/d\Omega_p)$ at each photon and proton angle. This is significant, in that in previous work [3,20] it was found that the shape of the coincident differential cross section has been most useful in comparisons with theoretical predictions. For a $1^+\rightarrow 0^+$ electromagnetic decay, the in-plane coincident cross section can be expressed as an angular correlation function, [3]

$$\frac{d^2\sigma}{d\Omega_p d\Omega_\gamma}(\theta_\gamma)=A(\theta_p)+B(\theta_p)\cos 2\theta_\gamma+C(\theta_p)\sin 2\theta_\gamma, \tag{13}$$

where θ_γ is the photon angle in the scattering plane, measured with respect to the $\hat{\mathbf{q}}$ direction [see Eq. (1)]. By fitting these three coefficients to the measured θ_γ angular distribution at each proton scattering angle, the relative shape of this coincident cross section, i.e., the size of the symmetric and antisymmetric (in θ_γ) pieces normalized to the isotropic piece, could be extracted as a function of θ_p for this transition. These ratios have the advantage of being independent of any overall normalization error and, in particular, are independent of any problems associated with beam integration.

Although the coincident yields we measured generally varied quite slowly with photon angle (this due to the low multipolarity of the decay process), concern over possible finite solid effects led us to investigate the sensitivity of the various $(\vec{p},p'\gamma)$ observables to the size of the angular integration region used to extract the photon yields. Given the geometry of the BaF_2 arrays (see Fig. 1) and because the yields were determined for each crystal individually in our analysis, it was possible to calculate spin observables based on the yields contained in just the seven inner crystals, thereby neglecting contributions from the twelve detectors on the perimeter of each array. The observables obtained using these smaller angular integrals were consistent within statistical errors with the values extracted by integrating the photon yield over the entire 19-pack. Because the latter case provided data of much higher statistical precision, we report those values for all observables in this work.

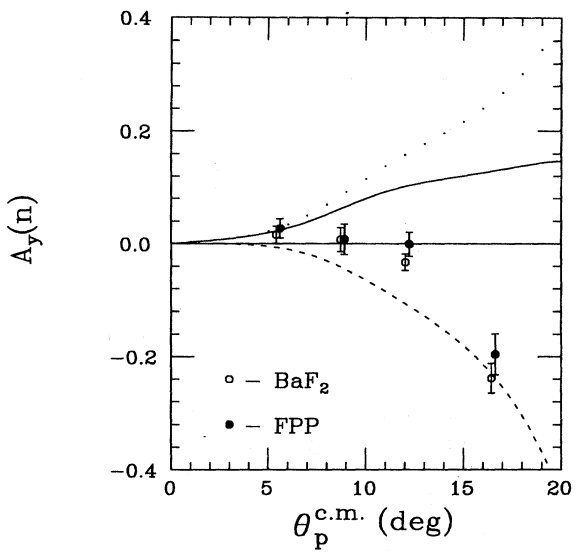

FIG. 9. Comparison of the normal-component coincident analyzing power $A_y(\hat{\mathbf{n}})$ and the combination of singles $(\vec{p},\vec{p}')$ observables given in Eq. (14), plotted versus $\theta_p^{c.m.}$. The calculations shown are described in the text.

It was pointed out previously that coincidence observables obtained when the photon is emitted normal to the scattering plane are sensitive to the same information that is contained in the normal-component $(\vec{p},\vec{p}')$ singles observables. More specifically, the normal-component coincident analyzing power can be expressed, in a model-independent manner [3], in terms of the $(\vec{p},\vec{p}')$ observables as

$$A_y(\hat{\mathbf{n}})=-\frac{(P-A_y)}{(1-D_{N'N})}. \tag{14}$$

Because we measured $A_y(\hat{\mathbf{n}})$ (with the BaF_2 array mounted directly above the scattering chamber) and all of the normal-component singles observables (using the FPP) simultaneously in this work, we could check the internal consistency of these data sets. In Fig. 9 we present the measured values of the coincident analyzing power $A_y(\hat{\mathbf{n}})$ plotted as a function of the center-of-mass proton scattering angle $\theta_p^{c.m.}$. Also shown in this figure is the combination of $(\vec{p},\vec{p}')$ observables that appears in Eq. (14), deduced from FPP yields. The excellent agreement seen between these two completely independent measurements of the same physical quantity gives us confidence that our measurements of both $(\vec{p},\vec{p}')$ and $(\vec{p},p'\gamma)$ observables are reasonable and consistent. The calculations shown in the figure will be described in the following section.

Before comparing our data to the predictions of several theoretical calculations, we summarize in Tables I and II the

TABLE I. Summary of normal-component $(\vec{p},\vec{p}')$ and $(\vec{p},p'\gamma)$ observables.

	$\theta_p^{\text{c.m.}}=5.5°$	$\theta_p^{\text{c.m.}}=8.8°$	$\theta_p^{\text{c.m.}}=12.1°$	$\theta_p^{\text{c.m.}}=16.5°$
A_y	0.024±0.005	0.039±0.007	0.010±0.005	−0.109±0.009
P	0.011±0.011	0.025±0.014	0.036±0.013	0.081±0.023
$D_{N'N}$	−0.088±0.026	0.099±0.032	0.149±0.024	0.119±0.041
B/A	0.128±0.028	0.203±0.032	0.116±0.018	−0.088±0.020
C/A	−0.031±0.031	−0.030±0.036	−0.057±0.025	0.057±0.030
$A_y(\hat{\mathbf{n}})$	0.027±0.017	0.008±0.027	−0.001±0.021	−0.196±0.036
$A_y(\theta_\gamma^{\text{lab}}=60°)$	−0.013±0.017	−0.028±0.020	−0.008±0.013	−0.257±0.027
$A_y(\theta_\gamma^{\text{lab}}=100°)$	0.030±0.015	0.066±0.018	0.073±0.011	−0.153±0.020
$A_y(\theta_\gamma^{\text{lab}}=140°)$	0.067±0.017	0.111±0.021	0.054±0.013	−0.191±0.020

final values determined in this work for all of the observables at all four proton scattering angles. The observables are divided according to the orientation of the incident beam polarization: Table I lists those observables obtained with the incident beam polarized along the normal to the scattering plane, while Table II contains those measured with the incident polarization vector oriented to lie in the scattering plane. In these tables and in all the figures of observables that follow, the errors shown include contributions from both statistical and systematic uncertainties. The former dominate in all cases, except for the observable A_y, for which the two are comparable.

V. DISCUSSION OF DATA AND CALCULATIONS

In previous sections, we have described the procedures by which these measurements were made and the observables extracted, and laid out much of the formalism we will use to interpret these data. We now examine the momentum transfer dependence of these observables and compare the results with several theoretical models, in attempts to identify trends in the data that may point to weaknesses in the underlying theory.

A. Description of the calculations

The calculations to which the data in this work will be compared were generated using the computer codes DREX [34] and DW81 [35], which formulate the proton-nucleus scattering problem in the relativistic and nonrelativistic impulse approximations (RIA and NRIA), respectively. Both codes include distortion of the incoming and outgoing waves due to the nuclear potential and also allow for explicit calculation of exchange contributions (see below). In all of the calculations considered here, the relative weights assigned by Cohen and Kurath [36] for the allowed $1p$-shell density matrix elements were used to describe the transition between the ^{12}C ground state and 15.11 MeV 1^+ state. In the relativistic calculation, the radial parts of the wave functions were taken to be single-particle Dirac spinors, with Woods-Saxon shapes for both the vector and scalar terms. The parameters of these potential wells are adjusted to yield proton orbitals that are consistent with electron scattering data [37]. Similarly, the radial pieces of the wave functions used in DW81 also have Woods-Saxon forms and describe the electron scattering data, but in this case are represented by single-particle Pauli spinors.

Before describing the form of the interaction used in each calculation, it is useful to clarify a few points concerning the role of exchange. In the impulse approximation, one assumes that a single interaction, often taken to be the free NN interaction, results in the transfer of energy and momentum from an incident (beam) nucleon to one of the target nucleons. One of these nucleons leaves the target and is detected; the other remains bound, with a wave function appropriate for the final (excited) nuclear state. Classically, one can think of "direct" processes as those in which the detected nucleon came originally from the beam, while in an "exchange" process, the beam nucleon becomes bound and the detected nucleon was found initially in the target. Quantum mechanically, of course, one cannot distinguish between the two processes; but within the context of a given model, one can evaluate overlap integrals appropriate for the different regions of momentum transfer involved (generally low q for direct processes, higher q for exchange). Attempts to parametrize free NN scattering in terms of direct and exchange contributions face a similar challenge, in that this separation can only be carried out in the context of a particular (e.g., meson-exchange) model. In either formalism (relativistic or nonrelativistic), nonlocal terms must be present if the interaction is to be able to reproduce the known features of free

TABLE II. Summary of in-plane-component $(\vec{p},\vec{p}')$ and $(\vec{p},p'\gamma)$ observables.

	$\theta_p^{\text{c.m.}}=5.5°$	$\theta_p^{\text{c.m.}}=8.8°$	$\theta_p^{\text{c.m.}}=12.1°$	$\theta_p^{\text{c.m.}}=16.5°$
D_λ	0.203±0.019	0.070±0.025	0.220±0.025	0.473±0.031
D_σ	−0.062±0.019	−0.004±0.022	0.087±0.025	0.185±0.031
$D_{0L}(nK)$	0.006±0.017	0.060±0.024	−0.013±0.025	0.007±0.038
$D_{0L}(nq)$	−0.039±0.012	−0.096±0.017	−0.127±0.018	−0.141±0.031
$D_{0S}(nK)$	−0.035±0.017	−0.028±0.022	0.015±0.028	0.176±0.039
$D_{0S}(nq)$	0.029±0.012	−0.004±0.015	0.043±0.019	0.223±0.030

NN scattering, especially at energies below several hundred MeV.

For the NRIA (DW81) calculations presented here, the elementary *NN* t matrix used was the phenomenological parameterization of Love and Franey [38], in which the interaction is written in terms of central, spin-orbit, and tensor terms, adjusted to reproduce the *NN* phase shift solutions of Arndt and Roper [39]. Because the t matrix in this case contains both direct and exchange components, it is manifestly nonlocal. For relativistic calculations, on the other hand, the lower components of the Dirac spinors used in this formalism already provide sufficient nonlocality that one can reasonably consider using a free *NN* interaction which does not include explicit exchange terms. We have therefore generated two sets of relativistic predictions for each observable. For one set, we have used a RIA which accounts for nuclear distortions (DRIA) [40], but in which knock-on exchange processes are not treated explicitly. For this calculation, the *NN* t matrix used is a sum-of-Yukawas fit [40] to the relativistic invariant *NN* amplitudes, determined from the same phase shifts as the Love-Franey description. No attempt was made in this case to separate the interaction into direct and exchange terms. For the second set of relativistic calculations, we used the full DREX prescription [34], in which exchange enters explicitly. Here, we used the direct-plus-exchange fits of Horowitz [41] to the invariant *NN* amplitudes to describe the interaction. We stress that for *each* of these calculations, the t matrix used represents the *full NN* amplitude. However, we have not examined the sensitivity of these calculations to the particular *NN* interaction used, either by considering, for example, various potential models or by adjusting interaction parameters to reproduce alternate sets of phase-shift solutions.

Our main point in the preceding discussion is to emphasize the consistency in these three treatments, in that calculations that consider only direct scattering processes (DRIA) use a direct-only parametrization of the full *NN* t matrix, while impulse approximations formulated to include knock-on exchange contributions (DW81 and DREX) use t matrices which have been separated into their direct and exchange components. Without such consistency, it is difficult to gauge reliably the importance of exchange processes for specific reaction observables. These ideas are illustrated quite clearly in Fig. 9 where, as noted earlier, the agreement between two independent experimental determinations of the same observable strongly supports the validity of the data. In this figure, we present three RIA calculations: the full DREX calculation, using a direct-plus-exchange parametrization of the *NN* interaction (solid line); a DRIA calculation (no exchange) using a direct-only *NN* interaction (short-dashed line); and a DRIA calculation, also no exchange, but using an interaction separated into direct and exchange components (dotted line). It is curious that the calculation which assumes (consistently) that only direct scattering contributes is able to describe the data better than the DREX calculation which allows for both direct and exchange processes, since exchange processes *must* contribute to this reaction at some level. We will return to this point below. For now, we observe that the "inconsistent" calculation (dotted line) does a markedly poorer job at describing the data than either of the first two. We note in passing that this last curve would result if one simply "turned off" the exchange option in the DREX code, but did not use a consistent (direct-only) parametrization of the interaction [34]. We also point out that this single curve in Fig. 9 represents the only calculation shown in which the t matrix used does *not* represent the full *NN* amplitude.

It is also possible to investigate the sensitivity of the observables measured in this work to the potential used to generate the incoming and outgoing projectile distorted waves. For each of the calculations plotted in Fig. 9, the distorted waves were generated "self-consistently," in that the free nucleon-nucleon interaction that was used to induce the transition is also folded with the ^{12}C ground state density (as determined from electron scattering data [42]) to produce the distortions of the four-component free Dirac spinors. Alternatively, one can generate the distorted waves using an optical model potential, with parameters adjusted to reproduce elastic scattering data. In the comparisons to our data that follow, we present DREX [34] and DW81 [35] calculations in which both methods for including nuclear distortion have been used. In each case, the optical model parameters were obtained [43] from fits to $p+^{12}$C elastic scattering differential cross section and analyzing power data taken at 200 MeV at IUCF [44]. Although data for the spin rotation function Q [45] were not included in the fitting process, the fits were later shown to be consistent with these data as well. The optical potential used in the relativistic code DREX was parametrized in terms of complex vector and scalar potentials, which were then inserted into the Dirac equation. For the nonrelativistic code DW81, "Schrödinger-equivalent" potentials were derived from the Dirac potentials just discussed. These potentials, when used in the standard Schrödinger equation (but with relativistic kinematics), yielded the same nucleon-nucleus phase shifts that resulted from use of the vector and scalar potentials in the Dirac equation.

In each of the remaining figures, we compare our measured values for the observables to the predictions of five calculations: two calculations generated by DW81 (NRIA with exchange), in which the distortions are generated either self-consistently (dotted line) or with "Schrödinger-equivalent" optical potentials (dot-dashed line); two calculations generated by DREX (RIA with exchange), in which the distortions are also generated either self-consistently (solid line) or using optical-model parameters as described above (long-dashed line); and a "direct-only" DRIA calculation (no exchange in the reaction model or in the parametrization of the *NN* t matrix), using self-consistent distortions (short-dashed line). A general observation is that while the calculations generated by DREX appear to be relatively unaffected by the type of distortion employed, the nonrelativistic calculations are significantly more sensitive to the choice of distorting potential.

B. Normal-component observables

We first examine the observables obtained with the incident beam polarized normal to the scattering plane. In the upper graph of Fig. 10, the $(\vec{p},p')$ reaction analyzing power A_y is plotted versus $\theta_p^{\text{c.m.}}$, along with the five calculations described above. As was found earlier for the normal-component coincident analyzing power $A_y(\hat{\mathbf{n}})$ (see Fig. 9), the direct-only relativistic calculation describes A_y reason-

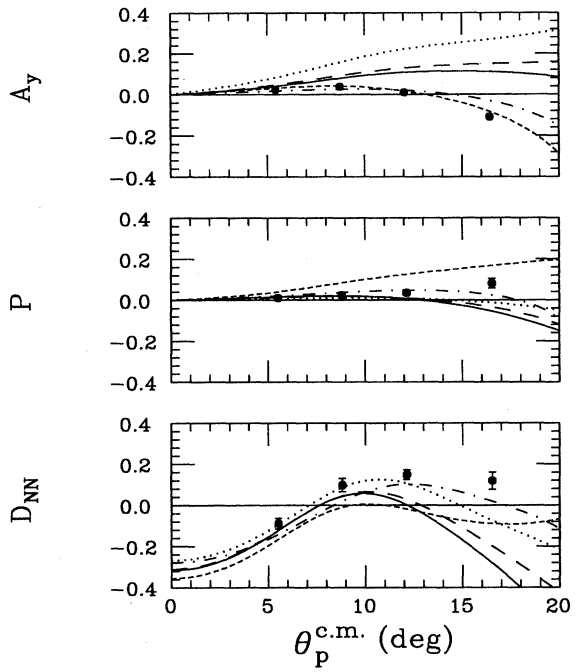

FIG. 10. Normal-component $(\vec{p},\vec{p}')$ spin observables A_y, P, and $D_{N'N}$, plotted versus $\theta_p^{c.m.}$. The five calculations shown, described in detail in the text, are DW81 with exchange, using self-consistent (dotted line) or optical model (dot-dashed line) distortions; DREX with exchange, using self-consistent (solid line) or optical model (long-dashed line) distortions; and "direct-only" DRIA using self-consistent distortions (short-dashed line).

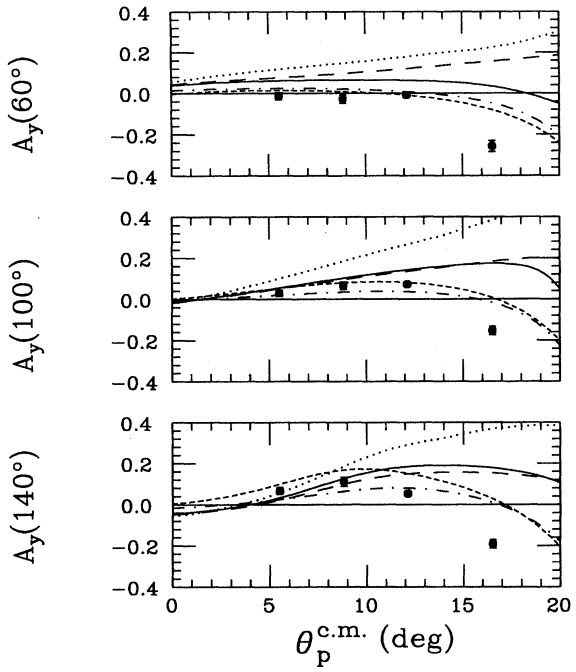

FIG. 11. Normal-component $(\vec{p},p'\gamma)$ coincident analyzing powers at $\theta_\gamma^{lab}=60°$, 100°, and 140°, plotted versus $\theta_p^{c.m.}$. The calculations shown are described in the caption of Fig. 10.

ably well, whereas the relativistic calculations that include both direct and exchange contributions (with either type of distortions) do not. Also, the nonrelativistic calculation using an optical-model-generated distorting potential does a much better job at describing this observable than does the DW81 calculation with "self-consistently" generated distortions. These same features can be seen in the calculations for the three remaining normal-component coincident analyzing powers $A_y(\theta_\gamma^{lab})$ (photon detected in-plane) shown in Fig. 11. Although these latter three observables are not described quite as well by the DRIA calculation and the DW81 calculation with optical-model distortions as is the singles analyzing power, the trend of the data to become more negative at larger $\theta_p^{c.m.}$ is followed by these two calculations. Again, it is curious that the relativistic calculations which incorporate both direct and exchange contributions cannot reproduce this pattern as well as the direct-only relativistic calculation.

Before discussing this observation in detail, we also examine the two other $(\vec{p},\vec{p}')$ singles observables that were measured using a vertically polarized beam: the induced polarization P and the normal-component spin-transfer coefficient $D_{N'N}$ (middle and lower graphs of Fig. 10, respectively). For each of these observables, all of the calculations shown exhibit very similar angle dependences, with the obvious exception of the DRIA calculation. This suggests that these two observables may also be sensitive to knock-on exchange processes. The induced polarization P is predicted to be small and take on negative values at larger $\theta_p^{c.m.}$ by all calculations which include exchange (though less so for the DWIA calculation with optical-model distortions), but is expected to increase to larger positive values by the DRIA calculation. The data show a slight preference towards the latter result, yet do not increase quite as rapidly with angle as this calculation would suggest. For $D_{N'N}$, the DREX calculations are completely wrong at the larger angles, and go negative much too soon, while DRIA does not go negative soon enough to be consistent with previous data taken at more backward angles [19] (see below). The nonrelativistic calculations do somewhat better and again demonstrate a clear preference for the optical-model generated distortions. It should be pointed out that the values of all three of the normal-component $(\vec{p},\vec{p}')$ observables measured in this work (Fig. 10) are consistent with the values obtained for these same observables in previous work at IUCF [19] which extended to higher momentum transfers.

To interpret these results, it is useful to note that by explicitly evaluating Eqs. (4) and (5) the induced polarization P and all five of the normal-component analyzing powers measured here (both singles and coincident observables) can be shown [30] to be sensitive to interferences between individual amplitudes in which both the proton and the recoil nucleus polarizations lie in the reaction plane. These same interference terms, which are expected [12] to be particularly sensitive to the nonlocal character (e.g., via exchange) of the NN interaction, can be isolated in the induced polarization and analyzing power difference $P-A_y$, which we have determined using two completely different techniques. Our final values for this quantity, along with the five calculations described earlier, are shown in Fig. 12. The data generally follow the same trend observed for $P-A_y$ at 150 MeV [10]

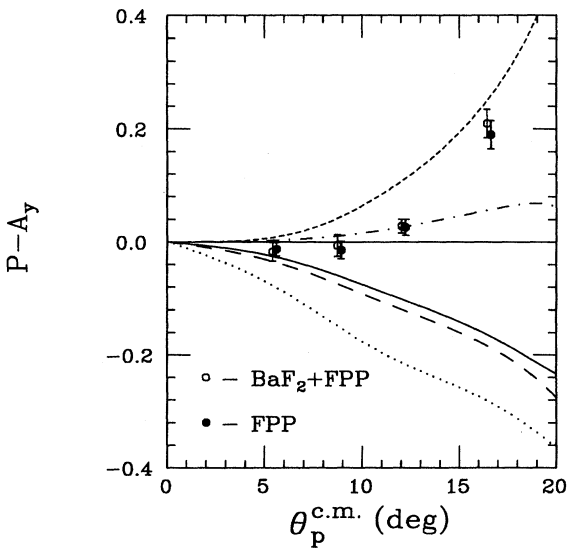

FIG. 12. $P-A_y$, determined using two independent techniques, versus $\theta_p^{\text{c.m.}}$. The calculations shown are described in the caption of Fig. 10.

and are seen to increase from small negative values at small momentum transfer to becoming large and positive at higher q. This trend is reproduced, at both energies, by the direct-only DRIA calculation, but not by the calculations that explicitly include exchange. Again, because exchange processes are expected to become more important as the incident energy decreases, this is a somewhat surprising result. Up at 400 MeV, on the other hand, the values measured for this quantity remain near zero over this entire momentum-transfer region [11], consistent with the expected decrease in strength of nonlocal processes at these higher energies.

This general feature, in which the direct-only DRIA calculation reproduces spin observables better than the full DREX result, has been noted in previous studies of this transition [17], and so it is useful to consider why this may be so. In order to properly include knock-on exchange processes in these calculations, the invariant amplitudes that characterize the free NN interaction must be broken up into direct and exchange components. This has been done for the calculations shown here using a simple meson-exchange model [41], for which it is sufficient to include only the "Born term," or first-order diagram, to obtain a complete representation of the free NN scattering process. While there may be valid concerns regarding the use of this same direct and exchange decomposition of the interaction within the nuclear medium (due, for example, to the momentum transfer dependence of mechanisms such as Pauli blocking that result in "effective interactions" or to account for the fact that the bound nucleons are necessarily off shell), these should not obscure the more important ambiguities and model dependence that are inherent in any attempt to separate the free interaction into direct and exchange terms [41].

If, on the other hand, the NN t matrix used is a reasonable approximation to the true interaction, then one must look for a deficiency in some other piece of the exchange calculation. Since the knock-on exchange scattering process necessarily imparts a large momentum transfer q to the struck nucleon, the wave function which describes the single-particle state of the target nucleon needs to be well described at high q in order for the exchange calculation to yield meaningful results. The relative weights assigned to the $1p$-shell single-particle transitions by Cohen and Kurath [36] have been shown [12] to be consistent with β-decay rate measurements ($q=0$) and provide a good description of the Gamow-Teller strength for (p,n) reactions and the $M1$ electromagnetic form factor for $q<1$ fm^{-1}. However, it is important to emphasize that all of these quantities are extremely insensitive to the strength assumed for the $LSJ=111$ component of the transition density [12,46] and can in fact be reproduced even if this term is eliminated entirely; yet $(\vec{p},\vec{p}')$ observables, such as P, A_y, and $P-A_y$, have been shown [8,9] to exhibit strong sensitivity to this particular spectroscopic amplitude at intermediate energies. Moreover, even if the relative weights of Cohen and Kurath are reasonable, they do not significantly constrain the radial part of transition density, especially at high q. Although the radial wave functions used in the calculations presented here yield results consistent with electron scattering data, the dominant contribution to these predictions comes from the large values of the potential wells in the interior region of the nucleus. Since the exchange parts of these calculations are sampling large momentum transfers, they are most sensitive to the tails of these radial wave functions, which are often difficult to extract from electron scattering data alone [46]. Changes in the large radius behavior of the wave functions (generated, for example, by choosing a different functional form for the radial dependence) would have a small impact on the quality of the fit to the electron scattering data, but could significantly change the exchange part of a proton-induced reaction calculation.

The final set of observables we obtained with the beam polarized normal to the reaction plane are those which characterize the coincident yields measured using the three BaF_2 arrays positioned in the scattering plane on beam right. Shown in Fig. 13 are the coefficients of the symmetric and antisymmetric (with respect to the momentum transfer direction $\hat{\mathbf{q}}$) terms of the in-plane coincident cross section, normalized to the isotropic piece [see Eq. (13)]. In this case, all of the curves shown appear to follow the data reasonably well, though the relativistic calculations do a somewhat better job describing the angular dependence of the observable B/A. All calculations, with the exception of the DW81 calculation using distortions generated in an optical model, predict a similar momentum-transfer dependence for C/A, which is qualitatively in agreement with the measured values of this quantity in this angular range. These two observables exhibited similar angular behavior at 400 MeV [20], but showed a more unambiguous favoring of the relativistic calculations at this higher energy.

C. In-plane-component observables

Six additional spin observables were determined from measurements of yield asymmetries when the incident beam polarization had been oriented to lie in the scattering plane. In Fig. 14, we present D_λ and D_σ, two linear combinations

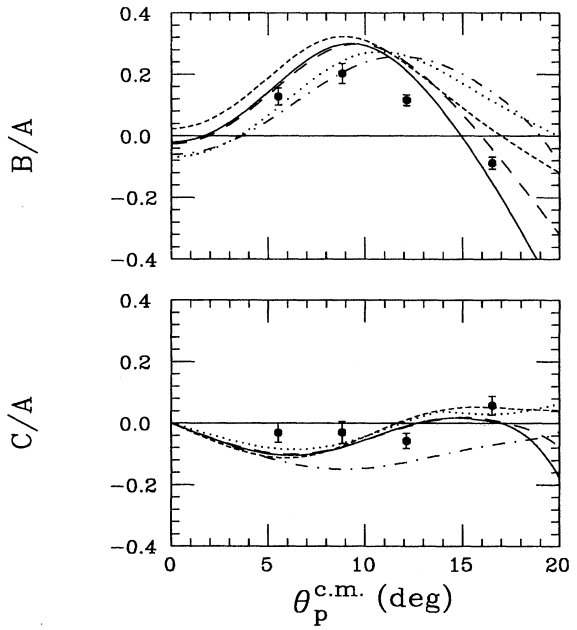

FIG. 13. Ratios of the symmetric (upper) and antisymmetric (lower) coefficients of the in-plane coincident cross section, relative to the isotropic term, as a function of $\theta_p^{c.m.}$. The calculations shown are described in the caption of Fig. 10.

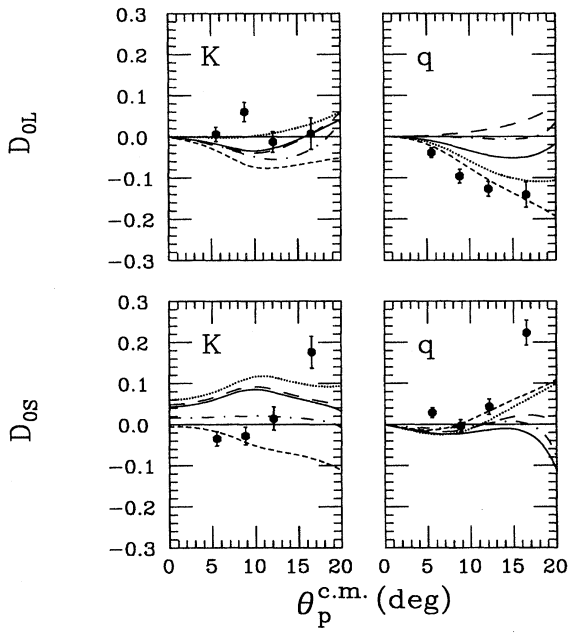

FIG. 15. Four coefficients describing the $(\vec{p},p'\gamma)$ coincident yield asymmetry measured 45° out of the scattering plane, plotted versus $\theta_p^{c.m.}$. The physical interpretation of each coefficient is provided in the text, while the calculations are described in the caption of Fig. 10.

of the four in-plane singles $(\vec{p},\vec{p}')$ spin-transfer coefficients, as defined in Eq. (10). We note that the momentum-transfer dependence of the observable D_λ (upper plot), which determines the asymmetry that would be measured at the FPP if

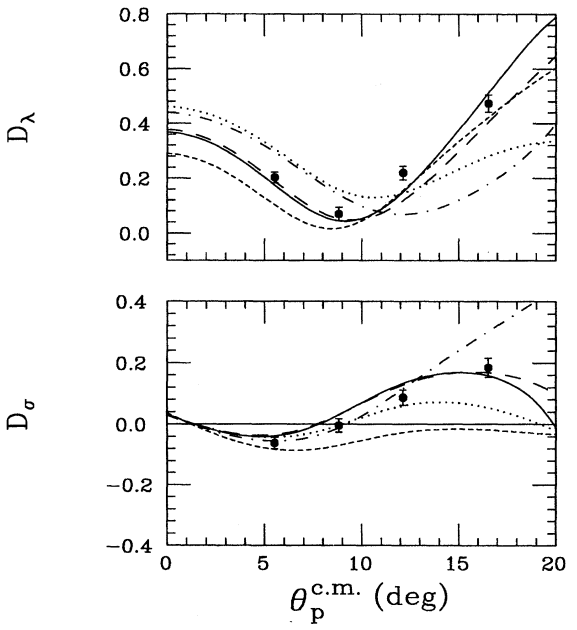

FIG. 14. D_λ and D_σ, two linear combinations of the four $(\vec{p},\vec{p}')$ in-plane spin-transfer coefficients [see Eq. (10)], plotted versus $\theta_p^{c.m.}$. The calculations shown are described in the caption of Fig. 10.

the incident beam was polarized purely along the longitudinal (beam momentum) direction [see Eq. (11)], is described significantly better by all of the relativistic calculations than by any of those based on a nonrelativistic formulation. The DREX calculations also reproduce the small-angle behavior slightly better than does the direct-only DRIA prediction. For D_σ (lower plot), which determines the FPP asymmetry for an incident beam polarized purely along the sideways direction, the DREX calculations again provide excellent agreement with the data at all values of momentum transfer. For both the relativistic and nonrelativistic calculations, however, there is a strong dependence at higher q on the form used for the distorting potential (more so for the DW81 calculations); data for this observable at larger angles would clearly be useful in selecting one DREX calculation, for example, over the other. As was observed for D_λ, the DRIA calculation is inferior in this case to either DREX prediction. Unfortunately, interpretation of these results is difficult, since each observable contains both diagonal and off-diagonal elements of the full spin-transfer matrix, as can be seen in Eq. (10). Measurements of these same quantities at a different value of the spectrometer spin precession angle α, a technique recently implemented at IUCF [47], would allow for a full decomposition of this matrix.

Finally, we present in Fig. 15 the four coefficients that describe the coincident $(\vec{p},p'\gamma)$ yield asymmetry measured in the cone 45° out of the scattering plane when the beam polarization vector lies *in* the reaction plane. The observables shown here are trivially related to the coefficients given in Eq. (12) (via a rotation in the scattering plane through the angle θ_{pK}), but their physical meaning may be better under-

stood from a more experimental point of view. These observables represent the asymmetries (due to reversal of the incident beam polarization direction) that would be measured if the beam were polarized purely along the longitudinal or sideways directions (upper or lower graphs, respectively) and if the photon were emitted in the average momentum ($\hat{\mathbf{K}}$) or momentum transfer ($\hat{\mathbf{q}}$) planes (left or right graphs, respectively). This unusual geometry, dictated by the form of the photon polarization tensor $t_{ij}(\hat{\mathbf{k}})$ given in Eq. (6), provides the only set of observables which are sensitive to the relative phases between the normal ($\hat{\mathbf{n}}$) and in-plane ($\hat{\mathbf{K}},\hat{\mathbf{q}}$) pieces of the scattering amplitude. As such, they are also the observables least constrained by previous studies of this or similar transitions.

In Fig. 15, we note that when the photon is emitted in the momentum-transfer plane (right-hand graphs), the direct-only relativistic calculation and the DW81 calculation using "self-consistently" generated distortions do reasonably well at describing the momentum-transfer dependence of both the sideways and longitudinal analyzing powers, although they miss the largest angle D_{0S} data point by approximately five standard deviations. When the photon is emitted in the ($\hat{\mathbf{K}}$) plane (left-hand graphs), on the other hand, none of the calculations even qualitatively describe the momentum-transfer dependence of these data over the entire angular range studied. Because these are the only observables that directly "connect" the phases of the normal and in-plane amplitudes, it is not obvious to what extent the parameters of the various calculations can be altered to improve agreement with these four coefficients, yet not disrupt predictions for other observables.

VI. SUMMARY AND CONCLUSIONS

We have carried out a program of simultaneous measurements of both $(\vec{p},\vec{p}')$ and $(\vec{p},p'\gamma)$ observables for excitation of the 15.11 MeV, 1^+, $T=1$ state in ^{12}C, at an incident beam energy of 200 MeV. These measurements include the first high precision determinations of the sideways and longitudinal analyzing powers D_{0S} and D_{0L} using the $(\vec{p},p'\gamma)$ reaction. Contained in this extensive data set (16 observables) is sufficient information, in principle, to allow for a complete determination of the scattering amplitude for this transition in a model-independent manner. By carrying out such a determination at each of the four scattering angles studied, the momentum dependence of these amplitudes may be mapped out.

Because every aspect of the scattering amplitude is probed by these data, they provide an extremely tight set of constraints on our theoretical models for this process. While several general features of the data and various calculations have been noted (e.g., the nonrelativistic DWIA calculations tend to exhibit more sensitivity to the choice of nuclear distorting potential than do the DREX predictions, with a clear preference for an optical-model parametrization adjusted to reproduce elastic scattering observables), the most intriguing result obtained is that the relativistic calculations which do not explicitly account for exchange, but use a (direct-only) interaction adjusted to reproduce the full NN amplitudes, appear to describe the data better than do the full DREX calculations, which include effects of knock-on exchange explicitly. This pattern is exhibited most clearly in all of the normal-component analyzing powers (both singles and coincident), as well as the quantity $P-A_y$, which is expected to be very sensitive to the nonlocal and exchange nature of the scattering process. This would suggest that there is a serious weakness in our present calculation of exchange terms in the relativistic models. Though this may be due at least in part to inadequacies in the interaction employed in the calculation, the observation of similar problems at higher energies might point to a shortcoming in the nuclear structure. One possibility is that the high q behavior of the radial wave functions is in error, since this is not well constrained by previous studies.

ACKNOWLEDGMENTS

We thank J. Piekarewicz and J. R. Shepard for providing us with the calculations and for insightful discussions regarding the physics contained in these calculations and their comparison with the data. Useful discussions with C. J. Horowitz are also appreciated. This work was supported in part by the U.S. National Science Foundation, under Grant No. PHY-9103794. Oak Ridge National Laboratory is managed by Lockheed Martin Energy Systems for the U.S. Department of Energy under Contract No. DE-AC05-84OR21400.

[1] See, for example, H. Baghaei, R. A. Lindgren, P. Slocum, E. J. Stephenson, A. D. Bacher, S. Chang, J. Lisantti, J. Liu, C. Olmer, S. Wells, S. W. Wissink, B. L. Clausen, J. A. Carr, S. K. Yoon, and F. Petrovich, Phys. Rev. Lett. **69**, 2054 (1992), and references therein.

[2] O. Häusser *et al.*, Phys. Rev. C **43**, 230 (1991).

[3] J. Piekarewicz, E. Rost, and J. R. Shepard, Phys. Rev. C **41**, 2277 (1990).

[4] A. Sudha Rao, K. S. Mallesh, and G. Ramachandran, Mod. Phys. Lett. A **7**, 175 (1992).

[5] G. Ramachandran, A. R. Usha Devi, and A. Sudha Rao, Phys. Rev. C **49**, R623 (1994).

[6] N. Mobed, S. S. M. Wong, and X. Zhu, Nucl. Phys. **A456**, 644 (1986).

[7] F. Ajzenberg-Selove, Nucl. Phys. **A506**, 1 (1990).

[8] J. R. Comfort, R. E. Segel, G. L. Moake, D. W. Miller, and W. G. Love, Phys. Rev. C **23**, 1858 (1981).

[9] J. R. Comfort, G. L. Moake, C. C. Foster, P. Schwandt, and W. G. Love, Phys. Rev. C **26**, 1800 (1982).

[10] T. A. Carey, J. M. Moss, S. J. Seestrom-Morris, A. D. Bacher, D. W. Miller, H. Nann, C. Olmer, P. Schwandt, E. J. Stephenson, and W. G. Love, Phys. Rev. Lett. **49**, 266 (1982).

[11] K. H. Hicks *et al.*, Phys. Lett. B **201**, 29 (1988).

[12] W. G. Love and J. R. Comfort, Phys. Rev. C **29**, 2135 (1984), and references therein.

[13] J. Piekarewicz, R. D. Amado, and D. A. Sparrow, Phys. Rev. C **32**, 949 (1985).
[14] J. R. Shepard, E. Rost, and J. A. McNeil, Phys. Rev. C **33**, 634 (1986).
[15] J. M. Moss, Phys. Rev. C **26**, 727 (1982).
[16] E. Bleszynski, M. Bleszynski, and C. A. Witten, Phys. Rev. C **26**, 2063 (1982).
[17] J. B. McClelland *et al.*, Phys. Rev. Lett. **52**, 98 (1984); X. Y. Chen, J. R. Shepard, M. R. Braunstein, T. A. Carey, K. W. Jones, J. B. McClelland, L. Rees, T. N. Taddeucci, N. Tanaka, and A. D. Bacher, Phys. Rev. C **44**, 2041 (1991).
[18] C. Olmer, in *Antinucleon- and Nucleon-Nucleus Interactions*, edited by G. E. Walker, C. D. Goodman, and C. Olmer (Plenum, New York, 1985), p. 261.
[19] A. K. Opper, Ph.D. thesis, Indiana University, 1991; A. K. Opper, S. W. Wissink, A. D. Bacher, J. Lisantti, C. Olmer, R. Sawafta, E. J. Stephenson, and S. P. Wells (unpublished).
[20] K. H. Hicks *et al.*, Phys. Rev. Lett. **61**, 1174 (1988).
[21] M. Kovash (private communication).
[22] C. R. Lyndon *et al.*, Phys. Rev. C **45**, 308 (1992).
[23] J. Piekarewicz and J. Shepard (private communication).
[24] See, for example, W. Haeberli, Annu. Rev. Nucl. Sci. **17**, 373 (1967).
[25] S. P. Wells, S. W. Wissink, A. D. Bacher, S. M. Bowyer, S. Chang, J. Lisantti, J. Liu, C. Olmer, A. K. Opper, T. Rinckel, and E. J. Stephenson, Nucl. Instrum. Methods A **325**, 205 (1993).
[26] G. P. A. Berg *et al.*, IUCF Scientific and Technical Report 1992–1993, p. 220.
[27] G. P. A. Berg *et al.*, IUCF Scientific and Technical Report 1986, p. 152.
[28] S. W. Wissink, in *Spin and Isospin in Nuclear Interactions*, edited by S. W. Wissink, C. D. Goodman, and G. E. Walker (Plenum, New York, 1991), p. 253.
[29] M. Thoennessen, J. R. Beene, F. E. Bertrand, and J. L. Blankenship, Oak Ridge National Laboratory progress report, 1989.
[30] S. P. Wells, Ph.D. thesis, Indiana University, 1994.
[31] S. M. Bowyer (private communication); S. M. Bowyer, S. W. Wissink, A. D. Bacher, T. W. Bowyer, S. Chang, W. Franklin, J. Liu, J. Sowinski, E. J. Stephenson, and S. P. Wells, in *Proceedings of the 11th International Symposium on High Energy Spin Physics*, edited by K. J. Heller and S. L. Smith (AIP, Woodbury, NY, 1995), p. 152.
[32] R. Novotny *et al.*, Nucl. Instrum. Methods A **262**, 340 (1987).
[33] GEANT computer codes, CERN Program Library Office, 1990.
[34] E. Rost and J. R. Shepard, computer code DREX (unpublished).
[35] R. Schaeffer and J. Raynal, Saclay Report No. CEA-R4000, 1970; modifications by J. R. Comfort.
[36] S. Cohen and D. Kurath, Nucl. Phys. **73**, 1 (1965); T. H. S. Lee and D. Kurath, Phys. Rev. C **21**, 293 (1980).
[37] E. Rost and J. R. Shepard, Phys. Rev. C **35**, 681 (1987).
[38] W. G. Love and M. A. Franey, Phys. Rev. C **24**, 1073 (1981); M. A. Franey and W. G. Love, *ibid.* **31**, 488 (1985).
[39] R. A. Arndt and D. Roper, Virginia Polytechnic Institute and State University Scattering Analysis Interactive Dialin (SAID) program and database.
[40] E. Rost and J. R. Shepard, Phys. Rev. C **40**, 1736 (1989).
[41] C. J. Horowitz, Phys Rev. C **31**, 1340 (1985).
[42] H. De Vries, C. W. De Jager, and C. De Vries, At. Data Nucl. Data Tables **36**, 495 (1987).
[43] P. Schwandt (private communication).
[44] H. O. Meyer, J. Hall, W. W. Jacobs, P. Schwandt, and P. P. Singh, Phys. Rev. C **24**, 1782 (1981).
[45] E. J. Stephenson, in *Antinucleon- and Nucleon-Nucleus Interactions*, edited by G. E. Walker, C. D. Goodman, and C. Olmer (Plenum, New York, 1985), p. 299.
[46] J. Dubach and W. C. Haxton, Phys. Rev. Lett. **41**, 1453 (1978).
[47] W. A. Franklin, A. D. Bacher, A. C. Betker, S. Chang, D. Prout, W. Schmitt, E. J. Stephenson, S. W. Wissink, and C. Yu, IUCF Scientific and Technical Report 1994–1995.